JOURNAL OF GEOPHYSICAL RESEARCH: BIOGEOSCIENCES, VOL. 118, 680–697, doi:10.1002/jgrg.20050, 2013

Hydrologic profiling for greenhouse gas effluxes from natural grasslands in the prairie pothole region of Canada

Irena F. Creed,[1] Johnston Miller,[1] David Aldred,[1] Jennifer K. Adams,[1] Salvatore Spitale,[1] and Rick A. Bourbonniere[2]

Received 16 August 2012; revised 15 March 2013; accepted 16 March 2013; published 13 May 2013.

[1] The prairie pothole physiographic region of North America is likely to be affected by climate change, and it is important to establish its baseline global warming potential as a basis for assessing global change effects. This study estimated the hydrologic effects on soil greenhouse gas efflux during the growing season along hydrologic profiles within natural prairie potholes ranging from the southern to northern limits of the prairie pothole region within central Canada. Soil moisture was found to be an important driver of differences in soil efflux along the hydrologic profiles and along the south-to-north gradient. The position of peak cumulative soil efflux varied along the hydrologic profile, with the N_2O peak occurring at the backslope, the CO_2 peaks at footslope and toeslope, and the CH_4 peaks at toeslope and surface waters. When cumulative soil efflux was converted to global warming potential (Mg CO_2 eq), the largest values were restricted to the narrow land-water interface in the south but expanded to a broader area of the hillslope in the north. CO_2 was the major ($> 95\%$) contributor to global warming potential. Omitting hydrologic controls on greenhouse gas fluxes from estimates of global warming potential led to substantial underestimates of the contributions of N_2O and CH_4. Arid regions in the south had smaller global warming potential than wetter regions in the north. If future climate projections for a warmer, drier climate in this region are realized, global warming potential from soil greenhouse gas fluxes will be smaller in this landscape, because the changing hydrologic conditions should result in a reduction of global warming potential from land surfaces, even as global warming potential from surface waters increases.

Citation: Creed, I. F., J. Miller, D. Aldred, J. K. Adams, S. Spitale, and R. A. Bourbonniere (2013), Hydrologic profiling for greenhouse gas effluxes from natural grasslands in the prairie pothole region of Canada, *J. Geophys. Res. Biogeosci.*, *118*, 680–697, doi:10.1002/jgrg.20050.

1. Introduction

[2] The prairie pothole region of north-central North America contains millions of freshwater wetlands, but more than 70% of Canadian [*Environment Canada*, 1986] and over 50% of American [*Mitsch and Gosselink*, 2000] wetlands have been lost to agricultural development. *Euliss et al*. [2006] estimate that the impact of wetland cultivation within the prairie pothole region is a 10.1 Mg/ha loss of soil organic carbon during the conversion to farmland. This represents a significant opportunity for carbon sequestration and subsequent greenhouse gas mitigation by restoring these wetlands. Although prairie pothole wetlands are important carbon stores [*Euliss et al*., 2006], the same conditions that cause organic carbon accumulation also produce the conditions under which other greenhouse gases such as methane (CH_4) and nitrous oxide (N_2O) are formed [*Badiou et al*., 2011]. This has led wetland restoration to become an issue of great interest in the field of climate change research.

[3] Prairie potholes store water in the form of ephemeral or permanent ponds of various size, shoreline complexity, and position along a large climatic gradient [*Johnson et al*., 2010]. Prairie pothole wetlands are usually disconnected from each other with respect to surface water drainage [*Winter and Rosenberry*, 1998; *Winter and LaBaugh*, 2003]. Wetland water balances are controlled primarily by snowmelt runoff and snowdrift from surrounding uplands, precipitation, and evapotranspiration. Groundwater in the deeper low conductivity till has only minor effects on the water balance [*Shieflo*, 1968; *Tiner*, 2003; *van der Kamp and Hayashi*, 2009]. The ponds are hydrologically dynamic, often losing considerable water volume and depth in seasonal responses to high evaporative stress and/or infiltration rates [*Johnson et al*., 2010]. The sensitivity and rapid response of these wetlands to environmental controls make them ideal microcosms in which to study the effects of climate on greenhouse gas storage and emissions, especially in the context of climate change [*Waiser*, 2006].

[1]Department of Biology, Western University, London, Ontario, Canada.
[2]Water Science and Technology Directorate, Environment Canada, Burlington, Ontario, Canada.

Corresponding author: I. F. Creed, Department of Biology, Western University, London, ON N6A 5B7, Canada. (icreed@uwo.ca)

2169-8953/13/10.1002/jgrg.20050

[4] Recent studies in the prairie pothole region have observed that hydrology plays a prominent role in determining the fate of carbon in restored wetlands [*Gleason et al*., 2009; *Millett et al*., 2009]. Prairie potholes comprise ponds surrounded by concentric bands of soils with water contents that vary in time and decrease with elevation [*van der Kamp and Hayashi*, 2009]. Potholes can be stratified into discrete spatial sampling units (e.g., crest, shoulder, backslope, footslope, and toeslope) that reflect differences in soil properties including soil moisture and soil temperature [*Pennock et al*., 1987]. The topographic pattern in soil water content downslope from the edge to the center of the pothole may be defined as the hydrologic profile of the pothole. Hydrologic profiles are important drivers of biogeochemical activity, including the production of greenhouse gas fluxes and the transport of greenhouse gas precursors from contributing source areas toward the ponds [*Yates et al*., 2006; *Phillips and Beeri*, 2008; *Gleason et al*., 2009]. *Dunmola et al*. [2010] found that hotspots (a relative term referring to topographic positions with relatively large global warming potential) of large CH_4 and N_2O emissions are localized to positions along hydrologic profiles and are driven by soil moisture and carbon availability. These findings are especially significant as drier climates may shift wetlands to more ephemeral states [*Niemuth et al*., 2010].

[5] The purpose of this study is to characterize the hydrologic controls on soil effluxes of carbon dioxide (CO_2), CH_4, and N_2O in the prairie pothole region on central Canada. The objectives are to (a) develop a technique for defining moisture and thermal profile features along contributing hillslopes of potholes; (b) use this technique to track soil effluxes of these gases along the environmental profiles and to identify the pattern of dominant controls on their formation over the growing season and at different spatial scales; (c) use this technique to aggregate global warming potential from the point to the profile feature to the pothole basin and to the parcel, and to compare the aggregated global warming potential along a geographic gradient from the prairie pothole region at the Canada-USA border to its northern limit in the Province of Saskatchewan; and (d) explore relationships between climate-driven controls and global warming potential so that we can predict changes in global warming potential in response to anticipated climate change in the region. These objectives are used to test the hypotheses that hydrologic profiles within potholes have a significant effect on soil greenhouse gas emissions. If this is indeed the case, incorporating hydrologically based monitoring of soil greenhouse gas emissions will lead to more accurate predictions of global warming potential in the prairie pothole region.

2. Study Area

[6] The prairie pothole region comprises a substantial portion of the Prairie Ecozone of central North America, covering approximately 800,000 km^2 (Figure 1). The prairie pothole region was formed during the Wisconsin glacial period through ice stagnations and thrusts that left a hummocky landscape upon retreat, resulting in millions of small closed basins commonly called potholes [*van der Valk and Pederson*, 2003]. Potholes range in size, depth, and connectivity, but the majority have a surface area < 1 ha and rarely become connected via surface water or groundwater hydrologic flow paths. The prairie pothole region of Canada covers four ecoregions that can reflect changes in climatic conditions: mixed grasslands, moist-mixed grasslands, aspen parkland, and boreal transition (Table 1). Grasslands occur across all four ecoregions.

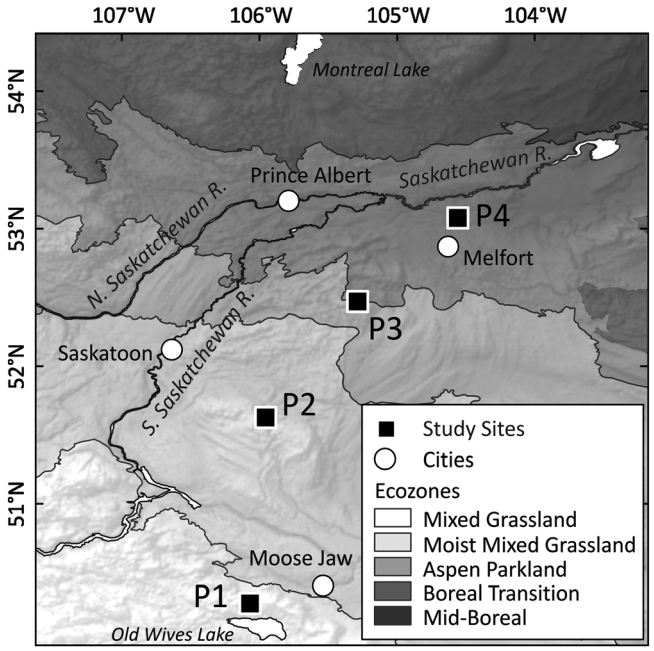

Figure 1. The prairie pothole region of North America and coarse-scale experimental gradient (P4 to P1) in Saskatchewan.

[7] This study was part of a collaborative research program studying landscape scale greenhouse gas dynamics in the prairie pothole region of Canada entitled "Finding a Natural Solution" [*Pennock*, 2007]. All study nodes were property of Ducks Unlimited Canada and subject to their management regimes. The program examined fluxes of CO_2, CH_4, and N_2O from soils in natural, restored, and managed prairie potholes. The current study focused on hydrologic dynamics that may influence greenhouse gas emissions in natural potholes, although there may be legacy effects of land use prior to restoration that may influence the distribution of soil nutrient pools, environmental conditions, and greenhouse gas efflux in the selected sites.

3. Methods

[8] Hydrologic profiles were examined at two scales. A fine-scale gradient was established based on a topographic template that reflects the different geomorphological and associated hydrologic and biogeochemical states driven by gravitational controls on water, sediment, and nutrient transport down a hillslope (Figure 2). For the coarse-scale gradient, four half-section parcels (P#) (i.e., 800 m × 1600 m) were selected in different ecoregions of the prairie pothole region along a moisture deficit transect to capture the range of soil moisture conditions from dry in the south (P1) to wet in the north (P4) (Figure 1b). The integration of both scales was explored by upscaling the topographically contained

Table 1. Characteristics of the Parcels (P1 to P4) That Form the Coarse-Scale Gradient[a]

	P1	P2	P3	P4
Longitude	−106.06	−105.95	−105.28	−104.55
Latitude	50.27	51.62	52.47	53.07
30 year mean annual temperature (°C)	3.7	2.5	1.9	1.4
30 year mean annual precipitation (mm)	378	441	433	394
30 year mean annual cumulative precipitation minus potential evapotranspiration (mm)	−151	−66	−61	−92
2006 mean temperature (°C)	5.2	3.5	2.8	2.7
2006 precipitation (mm)	485	561	725	489
2006 cumulative precipitation minus potential evapotranspiration (mm)	−118	−8	167	−56
Minimum elevation	688	598	552	398
Maximum elevation	717	627	571	408
Mean slope	8.7	10.1	6.2	5.0
Bedrock	Sandstone/shale	Sandstone/shale	Shale	Shale
Landform	Hummocky	Hummocky	Hummocky	Hummocky
Soil texture	Clay loam (moderately fine)	Clay loam (medium)	Silt loam (medium)	Loamy sand (moderately coarse)
Soil order	Dark brown chernozem	Dark brown chernozem	Dark gray chernozem	Dark gray hernozem
Mode of deposition	Till	Till	Lacustrine	Fluvial
Drainage	Well drained	Well drained	Well drained	Rapidly drained
Boreal subecozone	Mixed grassland	Moist-mixed grassland	Aspen parkland	Boreal transition
Upland vegetation: Grasses	*Stipa spp*. (Spear grass), *Bouteloua gracilis* (Blue gamma), *Buchloë dactyloides* (buffalo grass), *Agropyron spp*. (wheat grass)	*Festoca scabrella* (Fescue), *Stipa comata* (needle-and-thread), *Agropyron spp*. (wheat grass)		
Upland vegetation: Trees			*Populus tremuloides* (trembling aspen), *Populus balsamifera* (balsam poplar), *Quercus macrocarpa* (bur Oak)	
Wetland vegetation: Saline	*Spartina pectinata* (cord-grass), *Eleocharis palustris* (spike rush), *Panicum virgatum*, *Calamagrostis inexpansa* (northern reed grass), *Juncus balticus* (Baltic rush), *Solidago canadensis* (tall goldenrod)			
Wetland vegetation: Nonsaline	*Spartina gracilis* (alkali cord-grass), *Scirpus paludosus* (prairie bulrush), *Distichlis stricta* (alkali grass), *Puccinellia nuttalliana* (Nittall's alkali grass)			
Wetland vegetation: Trees	*Salix spp*. (Willow)			

[a]Mean annual climate data calculated for 1977 to 2006. Soil characteristics extracted from Soil Landscapes of Canada version 3.2 [*Soil Landscapes of Canada Working Group*, 2010]. Bedrock characteristics given in *Fung* [1969a]. Vegetation characteristics given in *Fung* [1969b] and *Scott* [1995].

hydrologic and biogeochemical responses for each parcel and then comparing these upscaled responses from relatively warm and dry to cool and wet conditions.

3.1. Topographic Classification

[9] A classification procedure was developed for assigning topographic features that were defined from fuzzy classification of terrain attributes derived from digital elevation models (DEMs) of the half-section parcels. The topographic features were defined as crests (CR) and shoulders (SH; upper convex slopes) in the upland positions, backslopes (BS) in the concave slopes between uplands and lowlands, and toeslopes (TS; flat area at the base of hillslopes) and footslopes (FS; moderately sloped transition between BS and TS) in the lowland positions. A flow chart of the topographic feature classification procedure is presented in Figures 3 and A1.

[10] Figure 3 summarizes the preparation of the DEM. First, 2.5 m (± 0.15 m vertical accuracy) DEMs were generated from light detection and ranging (lidar) data that were interpolated using an inverse distance weighted algorithm to 0.5 m and then resampled to 2.5 m using a bilinear resampling method [*Lindsay*, 2005]. A low pass 3×3 mean filter was then applied to smooth the effects of noise in the DEMs [*MacMillan*, 2000]. The filtered DEMs were then rescaled using a linear contrast stretch with no saturation to a fixed range of 0–25 m elevation to provide contrast in slope in parcels with very low relief (e.g., P4). Drainage channel networks were defined using a specific contribution area layer generated from a D8 flow algorithm on depression-filled DEMs. Channel initiation was set at a threshold of 8100 m^2 derived from visual assessment of the specific contributing area layer. Drainage basin boundaries and pond areas were surveyed on the ground at the beginning of the sampling periods with a Global Positioning System.

[11] Second, six terrain attributes were derived from the filtered and stretched DEMs: (1) percent height relative to local pits and peaks, (2) percent height relative to local channels and divides, (3) wetness index, (4) slope gradient, (5) profile curvature, and (6) plan curvature. For (1) and (2), relative positions were calculated using an eight direction flow algorithm (D8, which directs flow to the steepest downslope cell) [*O'Callaghan and Mark*, 1984]

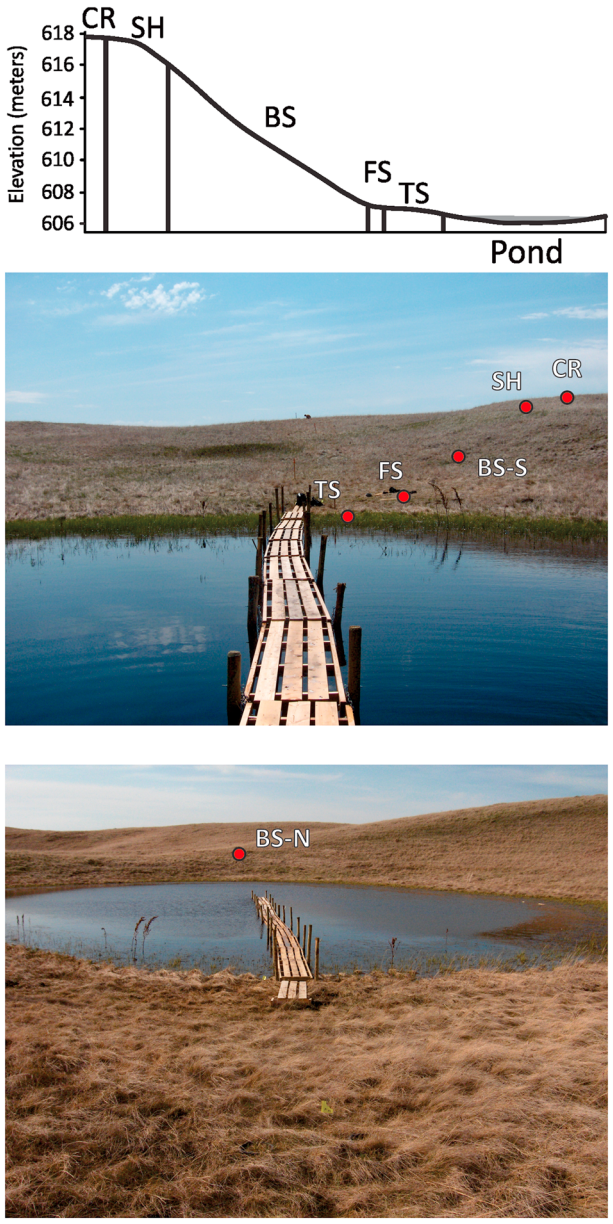

Figure 2. Fine-scale experimental gradient. Sampling stations were located along a south-facing topographic profile [crest (CR), shoulder (SH), backslope (BS-SF), footslope (FS), and toeslope (TS)] and on the backslope of the north-facing (BS-NF) slope of the Class 3 wetland. Soil carbon and nitrogen pools; moisture and temperature; and CO_2, CH_4, and N_2O effluxes were monitored at each sampling station.

on a DEM where single pits were removed (for pit to peak) and entire depressions were removed (for channels and divides) [*Planchon and Darboux*, 2002]. Topographic wetness index (3) was calculated as the natural logarithm of the specific contributing area using the infinite direction (Dinf) flow algorithm (which partitions flow to downslope cells proportional to the flow angle [*Tarboton*, 1997] divided by the local slope [*Beven and Kirkby*, 1979]). Slope gradient (4) was calculated as the rate of change of slope in the downslope direction on a 3×3 moving window [*Wilson and Gallant*, 2000]. Profile curvature (5) was calculated as the rate of change of slope in the downslope direction on a 3×3 moving window, with negative values for slopes increasing downhill (convex flow profile) and positive values for slopes decreasing downhill (concave profile) [*Wilson and Gallant*, 2000]. Plan curvature (6) was calculated as the curvature of a contour line formed by intersecting a horizontal plane with the surface, with negative values for horizontally concave profiles and positive values for horizontally convex profiles.

[12] Sample points for each topographic feature (i.e., CR, SH, BS, FS, and TS) were obtained from cross-section profiles of elevation from DEMs of the parcels. A total of 201 sample points were randomly divided into a training set of 99 samples and a testing set of 102 samples. Terrain attribute values at the training sample points were then extracted, and the statistical distributions of the terrain attribute values for each feature were compared to determine the appropriate attributes for separating features. A terrain attribute was considered to be useful for feature separation when the mean $\pm$ one standard deviation for a given feature was distinct from the means of other features or feature groupings [e.g., upland (CR, SH) or lowland (FS, TS)].

[13] Terrain attributes were modeled as fuzzy values between 0 (no feature membership) and 1 (full feature membership) using sigmoidal curve membership functions. The direction (increasing or decreasing) of the membership function was determined from the relationship of a given feature class mean to other feature class means (e.g., increasing if the given feature class mean was greater than the other feature class means). For an increasing function, the feature class mean value minus one standard deviation was used to define a membership score of 0.5, increasing to full membership at the mean. For a decreasing function, the feature class mean value plus one standard deviation was used to define a membership score of 0.5, decreasing from full membership at the mean. The arithmetic combinations of fuzzy membership values into fuzzy scores and the hierarchy of decision rules used to assign topographic features to the fuzzy scores are summarized in section A and Figure A1. Each rule assigns a topographic feature to a fuzzy score or passes the DEM grid cell unassigned to the next rule.

[14] The accuracy of this fuzzy classification procedure was assessed using the testing set of topographic feature sample points. Classification accuracies are presented in a confusion matrix that shows the instances of actual topographic features from the training sample points and the instances of topographic features predicted by the classification procedure. The overall accuracy of the classification model was 87.2% (Table 2). Each parcel had a similar distribution of features, with backslopes the dominant feature and the proportion of area increasing from crests to shoulders to backslopes, and then with small footslopes but significant toeslopes (Table 3).

3.2. Fine-Scale Gradient

[15] A pothole containing a seasonal wetland (typically dry by late summer) was selected within each parcel for instrumentation and monitoring during the growing season (1 May to 30 September) of 2006. Measurements were taken at five topographic features (CR, SH, BS, FS, and TS) along south-facing transects (Figure 2). The features were identified from classified maps and confirmed by ground survey.

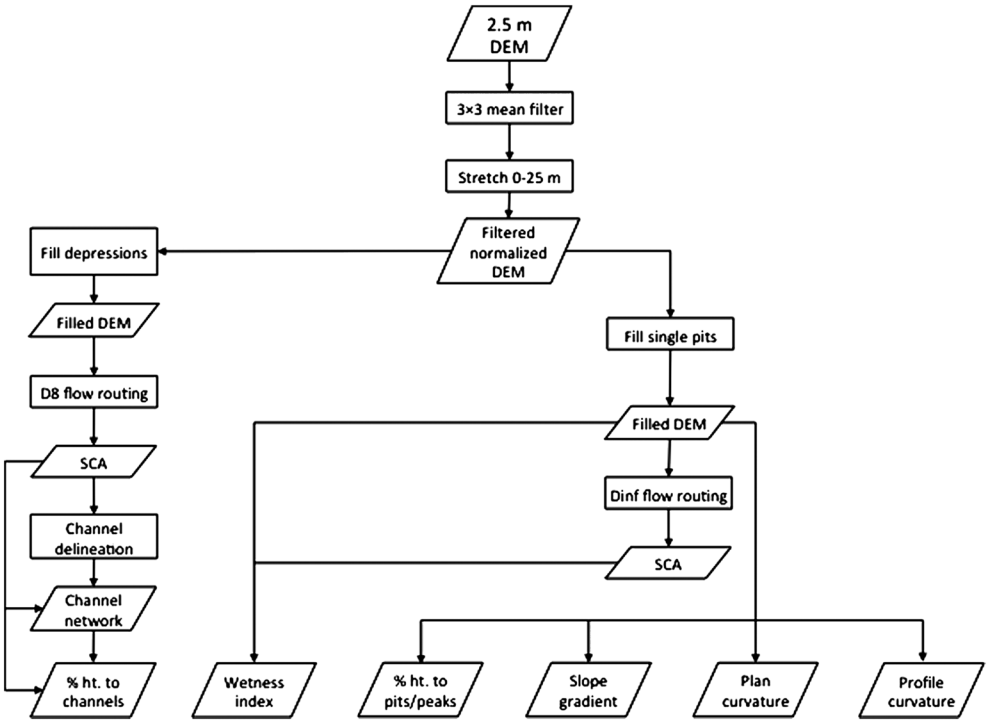

Figure 3. Flowchart of digital terrain analysis steps for deriving topographic attributes.

Both north and south facing BS features (BS-N and BS-S) were sampled to determine if there was a significant effect of slope aspect on soil properties. Soil carbon and nitrogen pools were sampled once at the beginning of the growing season, and soil moisture and temperature; soil CO_2, CH_4, and N_2O effluxes; and open water CO_2, CH_4, and N_2O effluxes were sampled weekly until the end of the growing season. Details of sampling methods are provided below.

3.2.1. Hydrologic Profiles

[16] Soil and pond water temperatures (top 6 cm) were measured using a digital thermometer. Soil moisture measurements (top 6 cm) were taken using a Delta-T ML2x ThetaProbe soil impendance (mV) probe (Delta-T Devices, Cambridge, UK) at each topographic feature. Five readings were recorded within a 1 m radius of each sampling point to account for local heterogeneity, and these readings were then averaged to obtain one representative reading per sampling site per sampling cycle and converted to volumetric soil moisture content using a calibration equation. Specifically, the volumetric soil moisture content of the 30 samples was determined gravimetrically by calculating the difference between initial wet weight and weight after oven drying, and a cubic polynomial regression model was then used to relate soil impedance readings to gravimetrically determined volumetric soil moisture in cm^3/cm^3 ($\theta = 2.02\ 10^{-9}\ x^3 - 2.47\ 10^{-6}\ x^2 + 1.11\ 10^{-3}\ x$ (where x is soil impedance); $r^2 = 0.94$; S.E. = 0.08; $p < 0.001$) [*Carlyle*, 2006].

3.2.2. Biogeochemical Profiles

[17] Soil carbon and nitrogen pools (0 to 10 cm; g/cm^2) were estimated from samples collected and composited from three replicates at each topographic feature using an open-faced soil corer. Samples were dried at 25°C and sieved, and then a subsample was analyzed for carbon (%)

Table 2. Confusion Matrix to Assess Accuracy of Classification of Topographic Features (CR = Crest; SH = Shoulder; BS = Backslope; FS = Footslope; TS = Toeslope) Within the Parcel[a]

		Observed					
		CR	SH	BS	FS	TS	%
Modeled	CR	7					100.0
	SH		16	1			94.1
	BS			26		1	96.3
	FS				12	3	80.0
	TS	1	1	4	2	28	77.8
	%	87.5	94.1	83.9	85.7	87.5	87.2

[a]For P2, the overall accuracy is 87.25%: the diagonal shows the number of grid cells that were assigned the same topographic feature in both observed and modeled approaches, omission errors correspond to nondiagonal column entries and are given as the omission accuracy per class in the bottom row, and commission errors correspond to nondiagonal row entries and are given as the commission accuracy per class in the right-hand column.

Table 3. Total Area (m^2) and Percentage (%) Area of Modeled Topographic Features per Parcel

	Area (m^2)	CR	SH	BS	FS	TS
P1	1,557,024	1.9	18.8	48.4	3.4	23.2
P2	1,230,662	1.5	19.9	47.4	3.3	18.4
P3	1,479,060	2.8	24.0	34.9	1.6	33.4
P4	1,311,196	1.6	30.7	44.7	3.5	15.0

and nitrogen (%) with a Carlo-Erba NA2000 analyzer (Carlo-Erba, Milan, Italy). Soil bulk density (0 to 10 cm) was estimated from samples collected using an Eijkelkamp Root Auger (Eijkelkamp, Zevenaar, Netherlands) with a drilling crown, dried at 105°C, and weighed for bulk density. Soil carbon and nitrogen pools were then calculated by multiplying the concentrations by bulk density to determine the pools within the top 10 cm of the soil surface.

[18] CO_2, CH_4, and N_2O effluxes were determined for each topographic feature and for the pond using the vented static chamber method [*Livingston and Hutchinson*, 1995]. For water, CO_2, CH_4, and N_2O effluxes were determined using three floating PVC chambers (19 cm ID, $V = 6.8$ l) that were placed on the water surface such that the bottom 3 cm was immersed, as close to the center of the pond as possible from a suspended boardwalk. For land, three replicate round PVC collars (19 cm ID) were installed at 10 cm depths at each topographic feature at the beginning of the sampling period. All chambers were insulated with reflective bubble wrap to minimize temperature change during the flux measurements. Plants within the collars were clipped 24 h prior to sampling to eliminate the effects of plant respiration on efflux measurements, meaning that our CO_2 efflux represents total soil respiration, which allowed us to focus on the effects of temperature and moisture on soil gas efflux. CO_2 efflux measurements were conducted using a portable PVC flux chamber (19 cm ID, $V = 11.3$ l) equipped with a mixing fan installed over the collars with a closed cell foam gasket, held in place by bungee cords, to create airtight seals. A CARBOCAP® GMP343 CO_2 Probe (Vaisala, Helsinki, Finland) infrared gas analyzer (IRGA) was used in conjunction with a Vaisala HMP75 T/RH probe to monitor changes in CO_2 concentration (ppmv), temperature, and relative humidity in the chamber, all of which were logged on a Vaisala MI-70 controller. CO_2 concentrations were corrected for temperature and relative humidity variations using compensation algorithms internal to the MI-70 software and recorded for 5 min in 15 s intervals.

[19] Smaller PVC chambers (19 cm ID, $V = 4.4$ l) and longer run times were used to determine CH_4 and N_2O fluxes because these were far smaller than CO_2 fluxes. Sampling tubing was attached to the chamber at one end and attached to a syringe at the other end. Ambient air samples (25 ml) were collected at each sampling location, and chamber air samples were collected at 20, 40, and 60 min by syringe and stored in 12.5 ml evacuated vials until analysis by gas chromatography. Separation was achieved on an SRI Instruments Model 8610C gas chromatograph (SRI Instruments, Torrance, CA, USA) using packed Haysep D columns and helium carrier. Detection for CH_4 was by flame ionization and for N_2O by electron capture.

[20] CO_2, CH_4, and N_2O effluxes were calculated as the slope of the linear regression relating gas concentrations in the chambers over time, then scaled according to the total volume (collar + chamber, with surface topography within the collar measured after the installation of each collar from the top of the collar to the soil surface to determine the total volume of air in the collar for soil effluxes), and corrected for ambient pressure and temperature. Mid-day soil effluxes ($\mu mol/m^2/s$) were determined between 0900 and 1500 local time, and the triplicate results were averaged for each topographic position. Daily soil efflux estimates ($g/m^2/d$) were made by scaling the average results for each position. Cumulative effluxes (g/m^2/growing season) were estimated by multiplying the daily effluxes by half the number of days between samplings (before and after) and summed over the growing season (1 May to 30 September 30).

[21] For soil respiration, all r^2 values were greater than 0.95 except when flux was near zero. For CH_4 and N_2O, we used 0.7 as a cut-off regression r^2. This was from either three or four points; in other words, we removed a single outlier point when initial r^2 was < 0.7. We often had zero flux for CH_4 and N_2O. If the ambient concentration was

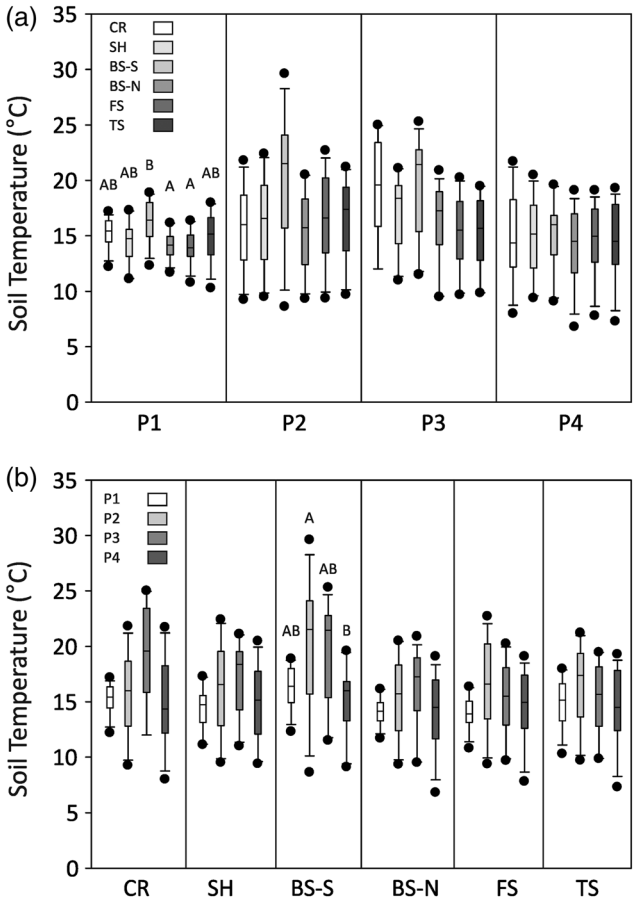

Figure 4. Median temperature sampled from topographic features from four parcels along a N-S longitudinal gradient (P4 to P1) during the growing season. Statistical differences (a) within parcels and (b) between parcels were assessed using one-way ANOVAs on ranks. Where significant differences were found ($p < 0.05$), Tukey tests were performed. Significant differences among features are shown with different letters. Where no significant differences are found between comparison groups, no letters are shown.

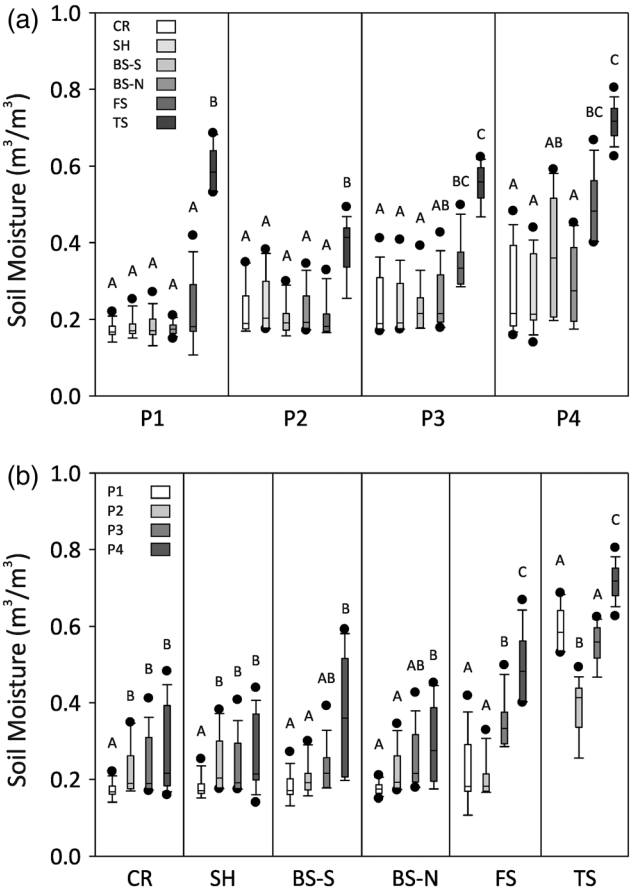

Figure 5. Median soil moisture sampled from topographic features from four parcels along a N-S longitudinal gradient (P4 to P1) during the growing season. Statistical differences (a) within parcels and (b) between parcels were assessed using one-way ANOVAs on ranks. Where significant differences were found ($p < 0.05$), Tukey tests were performed. Significant differences among features are shown with different letters. Where no significant differences are found between comparison groups, no letters are shown.

the same as the 60 min concentration, we called the flux "not significantly different from zero." We assigned a very small value as an estimate for zero (0.0001) to avoid problems with zeros in the statistical analysis.

3.3. Coarse-Scale Gradient

3.3.1. Hydrologic Profiles

[22] A coarse-scale gradient was established based on climatic conditions from the Canada-USA border to the northern limit of the prairie pothole region in Saskatchewan (Figure 1). A 400 km moisture deficit transect running through central Saskatchewan was interpolated from 30 year (1977–2006) meteorological data available from Environment Canada. Average annual moisture deficits were estimated from precipitation (P, mm/yr) *minus* potential evapotranspiration (PET, mm/yr), calculated using the method of *Hamon* [1961]. Four half-section parcels (P#) (i.e., 800 m 1600 m) were selected in the different ecoregions of the prairie pothole region and at intervals along the moisture deficit transect to capture the range of soil moisture conditions from dry in the south (P1) to wet in the north (P4) (Figure 1b). Geographical, meteorological, geological, topographical, and vegetation characteristics of each parcel are shown in Table 1. For each site, 2006 was a warmer and wetter year than the mean, although 2006 climate data fell within one standard deviation of their respective 30 year averages with the exception that precipitation at P3 in 2006 was the maximum of the 30 year time frame.

3.3.2. Biogeochemical Profiles

[23] Soil data in all topographic features and parcels were combined and used in models relating effluxes to soil temperature and moisture to determine the relative importance of soil moisture as a driver of potential differences in effluxes along the coarse-scale gradient.

3.3.3. Global Warming Potential

[24] Global warming potential was calculated as Mg CO_2 eq per ha (equivalent per hectare) per growing season for each type of topographic feature. The global warming potential of CO_2 could not be estimated using only efflux data because this

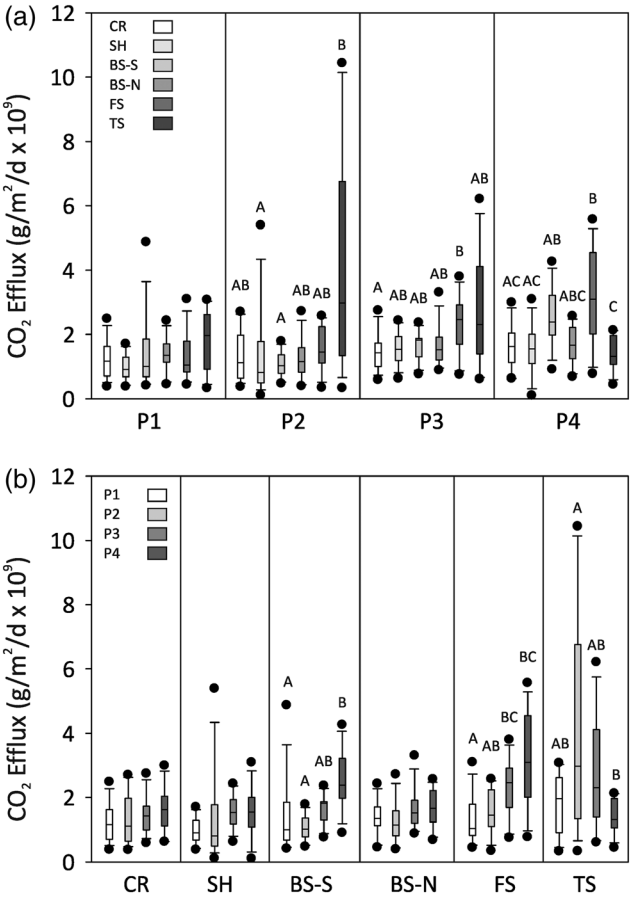

Figure 6. Median daily soil CO_2 efflux ($g/m^2/d \times 10^9$) sampled from topographic features from four parcels along a N-S longitudinal gradient (P4 to P1) during the growing season. Statistical differences (a) within parcels and (b) between parcels were assessed using one-way ANOVAs on ranks. Where significant differences were found ($p < 0.05$), Tukey tests were performed. Significant differences among features are shown with different letters. Where no significant differences are found between comparison groups, no letters are shown.

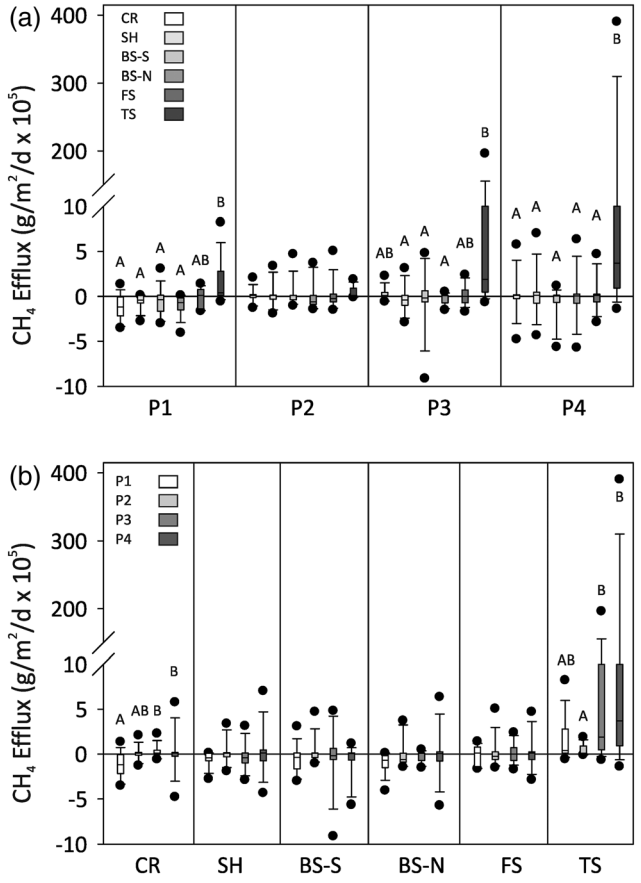

Figure 7. Median daily soil CH_4 efflux ($g/m^2/d \times 10^5$) sampled from topographic features from four parcels along a N-S longitudinal gradient (P4 to P1) during the growing season. Statistical differences (a) within parcels and (b) between parcels were assessed using one-way ANOVAs on ranks. Where significant differences were found ($p < 0.05$), Tukey tests were performed. Significant differences among features are shown with different letters. Where no significant differences are found between comparison groups, no letters are shown.

does not account for carbon sequestration. To estimate the global warming potential of CO_2, we used estimates of carbon sequestration from the literature and subtracted them from our CO_2 efflux data to give a net CO_2 exchange. For estimates of carbon sequestration, we used the results of *Nelson et al.* [2008], which determined the amount of CO_2 sequestered by comparing carbon stocks in cultivated versus restored wetlands at the footslope (2.34 g $C/m^2/yr \times 10^{10}$), mid-slope (1.86 g $C/m^2/yr \times 10^{10}$), and shoulder (2.04 g $C/m^2/yr \times 10^{10}$) topographic positions in the prairie pothole region. We used the data from the site that had been restored the longest (Vermillion, 9 years), because time since restoration can affect carbon sequestration rates (e.g., *Badiou et al.* [2011]). We also used data from *Badiou et al.* [2011] to estimate carbon sequestration in ponds based on soil organic carbon pools in the basins of long restored wetlands (1.15 g $C/m^2/yr \times 10^{11}$). In both cases, we assumed there would be negligible carbon sequestration during the dormant period (ground was frozen and/or covered with snow), allowing direct comparison with our data collected during the growing season. The amount of carbon sequestered was then converted into Mg CO_2 eq. For CH_4 and N_2O, the effluxes were converted into Mg CO_2 eq by multiplying by 25 and 298, respectively, using the 100 year time horizon from the Intergovernmental Panel on Climate Change [*Forster et al.*, 2007].

[25] To determine the global warming potential of a typical wetland in each parcel, the global warming potential per ha per feature was multiplied by a standardized area for each feature, determined by averaging the area of each feature type across parcels. To determine the total global warming potential of each parcel, the global warming potential per hectare was multiplied by the area of each feature, as determined by landscape classification. The global warming potential of each parcel was also standardized to P2 by multiplying the global warming potential of each feature by the area of each feature in P2.

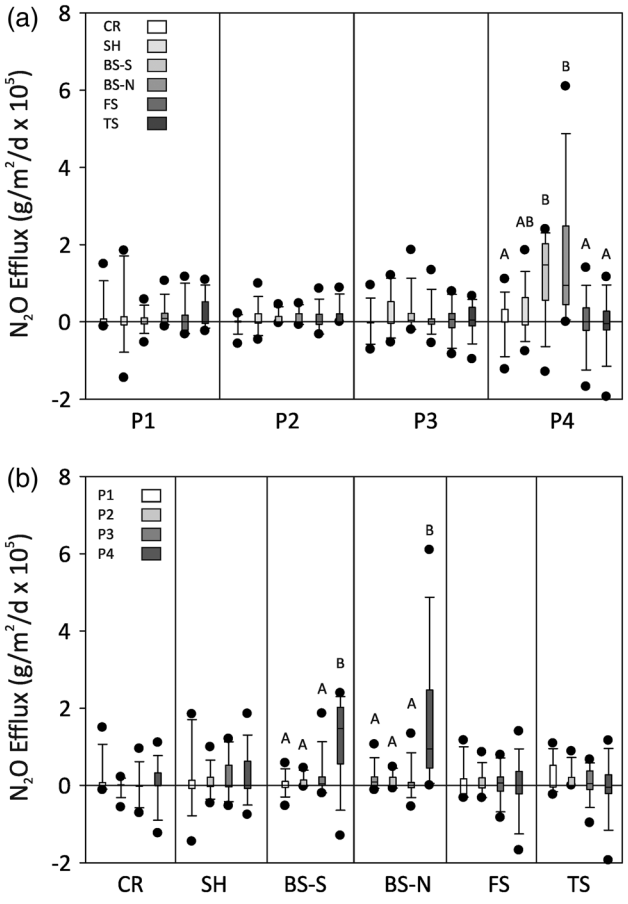

Figure 8. Median daily soil N_2O efflux ($g/m^2/d \times 10^5$) sampled from topographic features from four parcels along a N-S longitudinal gradient (P4 to P1) during the growing season. Statistical differences (a) within parcels and (b) between parcels were assessed using one-way ANOVAs on ranks. Where significant differences were found ($p < 0.05$), Tukey tests were performed. Significant differences among features are shown with different letters. Where no significant differences are found between comparison groups, no letters are shown.

Table 4. Properties of Soil Samples Composited From Three Replicates per Topographic Feature Compared Within Parcels (Across) and Between Parcels (Down)

	CR	SH	BS-S	BS-N	FS	TS	Across Transect
Carbon (g/m^2)							
P4	3870	2730	653	4310	5710	5970	4850 ± 1450
P3	2180	2590	290	2540	3670	N/A	2780 ± 5600
P2	5230	5620	475	3870	4230	4220	4650 ± 6700
P1	5350	6170	529	6410	8220	5850	6220 ± 1080
Across parcels	4090 ± 1290	4370 ± 1640	4940 ± 1010	4580 ± 1540	5950 ± 2070	5910 ± 1380	
Nitrogen (g/m^2)							
P4	322	267	603	349	506	520	428 ± 133
P3	229	299	239	227	289	N/A	257 ± 34
P2	214	169	269	240	281	315	248 ± 52
P1	401	558	480	534	699	478	525 ± 101
Across parcels	314 ± 91	350 ± 0.156	417 ± 157	371 ± 144	508 ± 225	493 ± 141	
C : N (molar)							
P4	12.0	10.2	10.8	12.3	11.3	11.5	11.4 ± 0.8
P3	9.5	8.7	12.1	11.2	12.7	N/A	10.8 ± 1.7
P2	24.5	33.3	17.6	16.1	15.1	13.4	20.0 ± 7.6
P1	13.3	11.0	11.0	12.0	11.8	12.2	11.9 ± 0.9
Across parcels	13.8 ± 6.2	14.7 ± 10.4	12.4 ± 3.0	12.6 ± 2.0	12.2 ± 1.8	12.2 ± 0.9	

[26] We determined the effect of spatial averaging on global warming potential estimates by comparing the six-feature models (CR, SH, BS, FS, TS, and pond) for CH_4 and N_2O to three models that combined different features. We used a "typical" prairie pothole with the areas of each feature representing the average across the four different sites (based on Table 3). For the four-feature model (CR + SH, BS, FS + TS, and pond), the cumulative fluxes for the combined features (CR with SH and FS with TS) were averaged and then multiplied by the combined area of the two features. The global warming potential of the four features were then added together to give a total global warming potential. For the two-feature model (CR + SH + BS + FS + TS and pond), the cumulative flux of the BS topographic feature was multiplied by the area of all the land topographic features and added with the pond feature to give a total global warming potential. For the one-feature model (CR + SH + BS + FS + TS + pond), the cumulative flux of the BS feature was multiplied by the total area of all six features to give a total global warming potential.

3.4. Statistical Analyses

[27] The statistical significance of differences (a) among different topographic features within a specific parcel or (b) among similar topographic features among different parcels were assessed using Mann-Whitney *U* tests between two values or Kruskal-Wallis one-way ANOVAs on ranks between multiple values where data were nonparametric. Where significant differences were found ($p < 0.05$), Tukey tests were performed. Soil effluxes were modeled in exponential relationships using a linear function of soil temperature and a quadratic function of soil moisture with linear offsets for carbon quantity and substrate quality [*Tang and Baldocchi*, 2005; *Webster et al*., 2009]. Each efflux was modeled using the general equation (1):

$$\ln R_s = y + a_1 T + a_2 M + a_3 M^2 + \varepsilon \quad (1)$$

where R_s is a soil efflux, T is soil temperature, M is soil moisture, a_i are fitted parameters, and ε is an error term described by parameterized linear offsets (Carbon pool and/or C : N). Forward stepwise regressions were performed for each model to examine the relative significance of each variable to the model's predictive ability. All statistical tests were performed in SigmaPlot ver. 12.0 [*Systat Software Inc*. 2011].

4. Results

4.1. Fine-Scale Gradient

[28] Hillslope transects represented hydrologic profiles through soil moisture distribution. Soil temperature showed no significant pattern among features along the hillslope transects (Figure 4a). Soil moisture tended to increase along hillslope transects from dry (CR) to wet (TS), although no significant differences were found among CR, SH, and BS features (i.e., uplands, including BS-N and BS-S). Soil moisture increased significantly in median FS and again in median TS in all parcels (Figure 5a). Soil moisture in TS features was significantly greater than CR, SH, and BS features in each parcel, while soil moisture in FS features was significantly greater than the higher elevation features in more northerly parcels P3 and P4 only.

[29] The following patterns emerged for daily soil efflux for CO_2, CH_4, and N_2O (Figures 6a, 7a, and 8a). For CO_2, a trend toward relatively larger median daily soil efflux could generally be observed from uplands (CR and SH) to lowlands (FS and TS) with relatively larger (> 150 kg/ha/d) values found at TS at P1, P2, and P3 and at FS at P2, P3, and P4, and significantly larger values at TS at P2 and P3 and at FS at P3 and P4 (Figure 6a). Similarly, for CH_4, significant increases and relatively large median daily soil efflux (positive values) occurred at FS and TS for P1 and P3 and at TS at P4 (Figure 7a). Finally, for N_2O, the median daily soil effluxes were much more heterogeneous, with significant increases and positive values found only at BS-S and BS-N at P4 (Figure 8a). Altogether, these observations suggest a hydrologically controlled profile of greenhouse gas soil efflux hotspots that shift from more narrow regions of the

Table 5. Median Daily Soil CO_2, CH_4, and N_2O Efflux (25%, 75%) Sampled From Aggregated Land Topographic Features and From Ponds From Four Parcels Along a N-S Longitudinal Gradient (P4 to P1) During the Growing Season[a]

CO_2 g/m^2/d	Land	Pond	p	CH_4 g/m^2/d	Land	Pond	p	N_2O g/m^2/d	Land	Pond	p
P4	1.8×10^9	2.3×10^8	<0.001	P4	1.1×10^4	8.3×10^6	<0.001	P4	1.6×10^3	-0.3×10^2	0.052
	(1.3×10^9, 2.4×10^9)	(1.7×10^8, 2.9×10^8)			(-2.3×10^4, 6.4×10^4)	(1.6×10^6, 1.3×10^7)			(0.0×10^3, 8.2×10^3)	(-2.2×10^3, 2.2×10^3)	
	A	A			A	AB			A		
P3	1.7×10^9	31.5×10^8	<0.001	P3	1.0×10^4	2.6×10^7	<0.001	P3	0.0	-0.2×10^2	0.397
	(1.3×10^9, 2.3×10^9)	(2.0×10^8, 3.5×10^8)			(-4.9×10^4, 5.8×10^4)	(1.0×10^7, 4.6×10^7)			(-0.5×10^2, 2.0×10^3)	(-2.3×10^3, 2.1×10^3)	
	AB	A			AB	A			AB		
P2	1.2×10^9	7.4×10^7	<0.001	P2	1.0×10^4	4.0×10^6	<0.001	P2	0.0	-0.5×10^2	0.137
	(8.0×10^8, 2.1×10^9)	(2.2×10^7, 8.4×10^7)			(-4.9×10^4, 1.0×10^4)	(7.5×10^5, 1.3×10^7)			(0.0, 1.6×10^3)	(-2.6×10^3, 1.6×10^3)	
	BC	B			AB	B			B		
P1	1.2×10^9	1.9×10^8	<0.001	P1	-2.6×10^4	1.8×10^7	<0.001	P1	0.0	-2.4×10^3	0.001
	(7.9×10^8, 1.7×10^9)	(1.7×10^8, 3.7×10^8)			(-12.8×10^4, 1.1×10^4)	(6.4×10^6, 2.7×10^7)			(-0.3×10^2, 1.7×10^3)	(-3.0×10^3, -0.8×10^2)	
	C	A			B	B			B		
p	<0.001	<0.001		p	0.006	0.023		p	0.001	0.372	

[a]Statistical differences between land and water profiles within parcels were assessed using Mann-Whitney U tests ($p < 0.05$). Statistical differences across parcels were assessed using Kruskal-Wallis one-way ANOVAs by ranks. Where significant differences were found ($p < 0.05$), Tukey tests were performed and significant differences among parcels are shown with different uppercase letters (vertically).

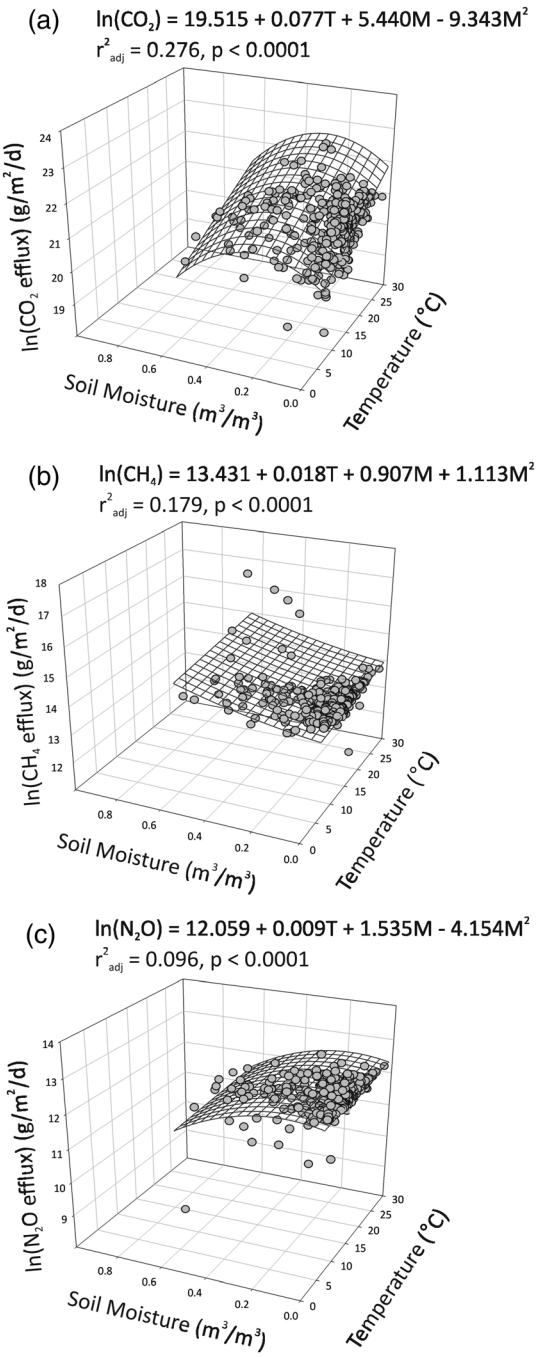

Figure 9. Observed efflux modeled as a function of soil temperature (T) and moisture (M) for (a) ln(CO_2), (b) ln (CH_4), and (c) ln(N_2O). Constants of 1,000,000 (CH_4) and 200,000 (N_2O) g/m^2/d were added to make the efflux values positive for the log transform.

hillslope that are most contiguous to the pond in the drier southern parcels to broader regions of the hillslope in the wetter northern parcels.

[30] Within parcels, carbon and nitrogen pools ranged from relatively small pools (CR and SH) to relatively large pools (TS), but with no clear trend in the ratio of C : N, which was generally less than 25 (Table 4). Therefore, soil moisture was a more important driver of potential

Table 6. Model of CO_2 Efflux ($g/m^2/d$) as a Function of Environment ($\ln(CO_2) = a + bT + cM + dM^2$, Where T = Soil Temperature (°C) and M = Soil Moisture (m^3/m^3)), C = Carbon Pool (g/m^2) and C : N Ratio for All Topographic Features

		Intercept	T	M	M^2	C	C : N	r^2	p
Environment	Coefficient	19.515	0.077	5.440	−9.343			0.276	<0.001
	Std. error	0.147	0.008	0.740	1.487				
	p	<0.001	<0.001	<0.001	<0.001				
Environment + C pool	Coefficient	19.427	0.079	5.470	−9.472	0.00001		0.275	<0.001
	Std. error	0.195	0.008	0.742	1.500	0.00002			
	p	<0.001	<0.001	<0.001	<0.001	0.492			
Environment + C : N ratio	Coefficient	19.850	0.077	4.950	−8.768		−0.022	0.308	<0.001
	Std. error	0.166	0.008	0.733	1.461		0.006		
	p	<0.001	<0.001	<0.001	<0.001		<0.001		
Environment + C pool + C : N ratio	Coefficient	19.672	0.080	4.976	−9.022	0.00003	−0.025	0.311	<0.001
	Std. error	0.198	0.008	0.732	1.466	0.00002	0.006		
	p	<0.001	<0.001	<0.001	<0.001	0.104	<0.001		

differences in soil effluxes along the hillslope transect than soil temperature or soil carbon and nitrogen pools.

[31] In comparison to the land, the pond exhibited the smallest median daily CO_2 efflux, the largest median daily CH_4 efflux, and about the same range as the other features for median daily N_2O efflux at all parcels (Table 5).

4.2. Coarse-Scale Gradient

[32] There were no consistent latitudinal trends in soil temperature moving from P1 to P4 (Figure 4b); soil temperature in uplands increased from P1 to P3 but with no general trend in the lowlands, while all features except BS-N and FS were coldest at P4. The only significant differences in soil temperature between parcels were found at BS-S, but these did not conform to a latitudinal trend.

[33] Meanwhile, the coarse-scale gradient represented a hydrologic profile from dry (P1) to wet (P4) at all features except TS where soil moisture was lower in P2 and P3 than P1 (Figure 5b). Soil effluxes appeared to follow the pattern of increasing along the latitudinal gradient from south to north, with median daily CO_2 efflux increasing in BS-S and FS features (Figure 6b), CH_4 efflux in CR and TS features (Figure 7b), and N_2O efflux in BS-S and BS-N features (Figure 8b), although no significant trends or differences were found in other features. The distribution of carbon and nitrogen along the hillslope transects also varied along the coarse-scale gradient. P1 contained the largest carbon and nitrogen pools (Table 4) but lowest median daily soil CO_2, CH_4, and N_2O effluxes among all five parcels (Table 5). In contrast, P2, P3, and P4 had smaller carbon and nitrogen pools but larger median daily soil CO_2, CH_4, and N_2O effluxes. The drier conditions in the south lead to greater accumulation of carbon and nitrogen pools but lower rates of transformation of these pools to greenhouse gas effluxes. Therefore, soil moisture is an important driver of potential differences in soil effluxes than soil temperature along the coarse-scale gradient from P1 to P4.

[34] Neither soil temperature nor soil moisture was found to explain much of the variance in exponential models developed from effluxes aggregated across hillslopes and parcels (Figure 9), although the relationships for each efflux were found to be significant. Linear offsets for carbon pools and C : N ratios improved the predictive ability of the CO_2 model (Table 6) although these variables were found to be less important than soil temperature and moisture (Table 9). The offsets failed to improve the predictive ability of the CH_4 and N_2O models (Tables 7–9). Soil moisture was found to be an important predictive variable for each model although soil temperature contributed to a greater portion

Table 7. Model of CH_4 Efflux ($g/m^2/d$) as a Function of Environment ($\ln(CH_4) = a + bT + cM + dM^2$, Where T = Soil Temperature (°C) and M = Soil Moisture (m^3/m^3)), C = Carbon Pool (g/m^2), and C : N Ratio for All Topographic Features[a]

		Intercept	T	M	M^2	C	C : N	r^2	p
Environment	Coefficient	13.431	0.018	0.907	1.123			0.179	<0.001
	Std. error	0.105	0.006	0.527	1.060				
	p	<0.001	0.002	0.086	0.290				
Environment + C pool	Coefficient	13.395	0.019	0.919	1.069	0.000006		0.177	<0.001
	Std. error	0.139	0.006	0.529	1.070	0.000015			
	p	<0.0001	0.002	0.083	0.318	0.688			
Environment + C : N ratio	Coefficient	13.450	0.018	0.880	1.154		−0.001	0.177	<0.001
	Std. error	0.121	0.006	0.535	1.066		0.004		
	p	<0.001	0.002	0.101	0.280		0.762		
Environment + C pool + C : N ratio	Coefficient	13.411	0.019	0.886	1.010	0.000007	−0.002	0.175	<0.001
	Std. error	0.145	0.006	0.536	1.074	0. 000016	0.004		
	p	<0.001	0.002	0.099	0.307	0.633	0.690		

[a]A constant of 1,000,000 was added to make all CH_4 efflux values positive for the log transform.

Table 8. Model of N_2O Efflux ($g/m^2/d$) as a Function of Environment ($\ln(N_2O) = a + bT + cM + dM^2$, Where T = Soil Temperature (°C) and M = Soil Moisture (m^3/m^3)), Carbon Pool (g/m^2), and C : N Ratio for All Topographic Features[a]

		Intercept	T	M	M^2	C	C:N	r^2	p
Environment	Coefficient	12.059	0.009	1.535	−4.154			0.096	<0.001
	Std. error	0.085	0.005	0.430	0.865				
	p	<0.001	0.054	<0.001	<0.001				
Environment + C pool	Coefficient	11.922	0.011	1.581	−4.355	0.00002		0.103	<0.001
	Std. error	0.113	0.005	0.430	0.869	0.00001			
	p	<0.001	0.023	<0.001	<0.001	0.066			
Environment + C:N ratio	Coefficient	12.102	0.009	1.471	−4.080		−0.003	0.096	<0.001
	Std. error	0.099	0.005	0.437	0.870		0.003		
	p	<0.001	0.054	<0.001	<0.001		0.381		
Environment + C pool + C:N ratio	Coefficient	11.967	0.011	1.492	−4.274	0.00003	−0.004	0.105	<0.001
	Std. error	0.118	0.005	0.435	0.870	0.00001	0.003		
	p	<0.001	0.020	<0.001	<0.001	0.038	0.189		

[a]A constant of 200,000 was added to make all N_2O efflux values positive for the log transform.

of the model's predictive ability for CO_2 and CH_4 but was not an important variable for the N_2O model.

[35] Cumulative soil fluxes can reveal signals not apparent in daily soil greenhouse gas effluxes. For this reason, the growing season cumulative soil effluxes along the hillslope transects were compared by parcel (Figure 10). Cumulative soil CO_2 effluxes typically increased from uplands (CR and SH) to lowlands (FS and TS) for all parcels with peak cumulative effluxes occurring at FS at P4 and at TS at the other parcels. Peak cumulative soil CH_4 effluxes were found at TS at P3 and P4, while there was no peak cumulative soil N_2O except at BS at P4. The lowest cumulative CO_2 and N_2O effluxes and largest cumulative CH_4 effluxes were found in ponds at all parcels. Cumulative global warming potential (Mg CO_2 equivalent) was heterogeneous, with the largest cumulative global warming potential typically found in the lowlands (FS and TS; Figure 11).

[36] The sensitivity of the model for calculating cumulative global warming potential for CH_4 and N_2O from the sum of global warming potentials in six topographic features (five on land plus the pond) for each parcel (i.e., the reference condition) was tested against estimates derived from the sums of global warming potentials calculated using the simplified aggregation schemes (Figure 12). Cumulative global warming potential contributions from CH_4 were underestimated by each of the aggregation schemes, and there was a large underestimation (> 100%) in the model using the dominant feature BS CO_2 equivalent global warming potential as the estimate for all features including ponds. Global warming potential contributions from N_2O were either underestimated or overestimated by each of the aggregation schemes, with estimates accounting for four features generally being the most accurate. These results emphasize the importance of using topographic features to map greenhouse gas effluxes, as each simplification of the aggregation scheme resulted in an increase in the error of estimating cumulative global warming potential, and errors were larger in the wetter northerly parcels.

[37] The relationship of P-PET versus total ($CO_2 + CH_4 + N_2O$) cumulative global warming potential (Mg CO_2 equivalent) was examined to determine if there was a trend in cumulative global warming potential along the coarse-scale gradient. The total global warming potential based on the sum of topographic features of each parcel is sensitive to both the distribution of topographic features and the moisture characteristics of the parcel. This simple arithmetic summing does not account for variation in total area of the different topographic positions among the different parcels; for example, the greenhouse gas "hotspot" lowland areas (FS and TS) ranged substantially among the parcels from a range of 22–27% of the total area in the southern parcels (P1 and P2) to 35% in P3 to a low of 18% in P4. To remove the sensitivity to the distribution of topographic features between parcels, a standardized total global warming potential was calculated for parcels using the distribution of topographic features found in P2. Both real total global warming potential and standardized total global warming potential showed increases with P-PET (Figure 13). Land features (i.e., CR, SH, BS, FS, and TS) were the major source of global warming potential, contributing over 99% of global warming potential. Some of the ponds were net sinks of global warming potential. CO_2 was the major

Table 9. Forward Stepwise Regression Analysis to Predict Gas Effluxes ($g/m^2/d$) From Environmental (Soil Temperature (T) and Soil Moisture (M)), Carbon Pool (C), and C : N Ratio Variables[a]

CO_2 Step	Variable	r^2	Δr^2	p	CH_4 Step	Variable	r^2	Δr^2	p	N_2O Step	Variable	r^2	Δr^2	p
1	T	0.155	0.155	<0.001	1	T	0.159	0.159	0.002	1	T	–	–	–
2	M	0.223	0.068	<0.001	2	M	–	–	–	2	M	0.034	0.034	<0.001
3	M^2	0.286	0.063	<0.001	3	M^2	0.183	0.024	<0.001	3	M^2	0.066	0.033	<0.001
4	C	0.326	0.039	<0.001	4	C	–	–	–	4	C	–	–	–
5	C : N ratio	0.338	0.013	<0.001	5	C : N ratio	–	–	–	5	C : N ratio	–	–	–

[a]Blank cells (–) indicate that the variable did not significantly add to the ability of the equation to predict effluxes.

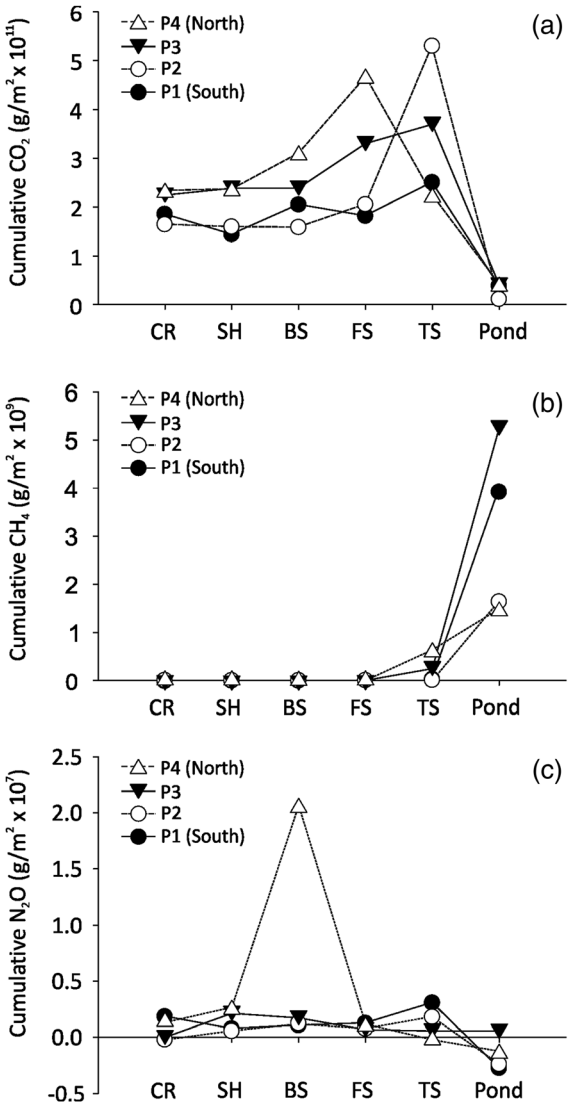

Figure 10. Cumulative greenhouse gas efflux for (a) CO_2 ($g/m^2 \times 10^{11}$), (b) CH_4 ($g/m^2 \times 10^9$), and (C) N_2O ($g/m^2 \times 10^7$) across topographic features (with north and south facing BS values averaged) for P1 (south) and P4 (north).

constituent in global warming potential with the trace gases CH_4 and N_2O together contributing < 3% to the global warming potential.

5. Discussion

[38] Wetlands in the prairie pothole region are predicted to undergo changes in number, area, and periodicity as a result of climate change [*Niemuth et al*., 2010]. However, it is uncertain how climate change will affect the carbon stores and emissions of greenhouse gases within these wetlands [*Bridgham et al*., 2006; *Phillips and Beeri*, 2008]. The net benefit of carbon sequestration in these wetlands in terms of a reduction in global warming potential has been questioned because of potentially greater emissions of greenhouse gases [*Badiou et al*., 2011]. Furthermore, there is a need to improve our understanding of changing hydrologic and thermal conditions on CO_2, CH_4, and N_2O emissions from natural wetlands [*Gleason et al*., 2009].

[39] In this study, we tested the hypothesis that topographically defined hydrologic and/or thermal profiles are an important influence on soil greenhouse gas fluxes in prairie pothole basins. Within the relatively flat landscapes, we designed a spatially explicit topographic template that distinguished hillslope features using digital terrain analysis techniques. The potential for hydrologic and/or thermal controls on greenhouse gas efflux was explored along these topographic profiles across a broad climatic gradient, where growing season soil moisture ranged from 0.107 to 0.805 m^3/m^3 and soil temperature from 6.8 to 29.6°C. Soil moisture was found to be the primary control on effluxes along hillslope transects. Along the climatic gradient, soil moisture was consistently lower in the southern transect (P1) compared to the northerly sites (e.g., P4) across almost all topographic features from CR to TS, while soil temperature showed no consistent differences either among parcels or among features. Soil moisture was found to be a significant driver of potential differences in effluxes among all topographic features across the climatic gradient, although soil temperature was also found to play a role in the predictive ability of models relating CO_2 and CH_4 effluxes to environmental variables across different geographies. However, the overall poor predictive abilities of these models and the lack of a trend in soil temperature along the climatic gradient suggest that effluxes across different geographies may also be responding to other physiographic differences that have not been accounted for, such as soil types and drainage properties.

[40] The main contributor to global warming potential was CO_2. The important role of CO_2 in greenhouse gas emission has been observed in recent studies, both in cultivated and noncultivated areas of the prairie landscape [e.g., *Gleason et al*., 2009]. In this study of natural areas, larger cumulative CO_2 fluxes were found in northern parcels, and smaller CO_2 fluxes were found in the southern parcels. Currently, these parcels do not have consistently greater soil organic carbon; however, over time the pools of soil organic carbon in the northern parcels may become depleted by soil respiration at a faster rate than those in the southern parcels. The relatively wet conditions in northern parcels may enable carbon cycling, whereas soil organic carbon may be more likely to be stored in the relatively dry conditions that existed during the study period and in recent years [*Brye and Gbur*, 2010]. It must be noted that the carbon sequestration rates were estimated literature values from cultivated versus native land use comparisons [*Nelson et al*., 2008; *Badiou et al*., 2011] within the prairie pothole region. Even though these estimates are from the same region, they do not capture the variation among the sites and may not accurately represent the amount of carbon sequestered in this area. More accurate estimates of the carbon sequestered in the different sites would give a clearer picture of the global warming potential of the wetlands in the prairie pothole region.

[41] The trace gases N_2O and CH_4 were minor contributors to global warming potential but also showed patterns in response to the hydrologic profile. Cumulative soil CH_4 effluxes occurred in appreciable amounts only at the wettest topographic features (TS) and particularly in the inundated

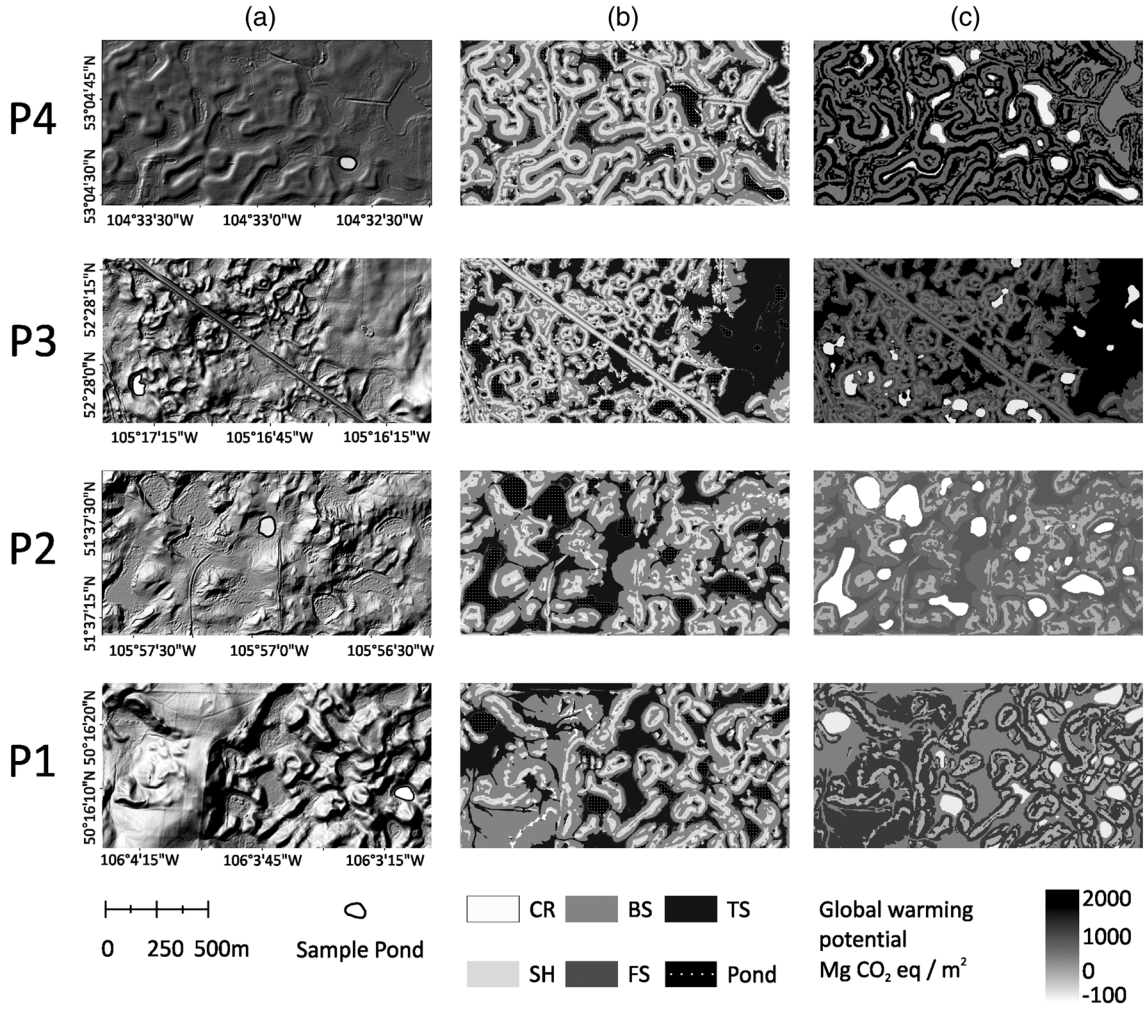

Figure 11. For each of the parcels, (a) a 2.5 m LiDAR digital elevation model (DEM), (b) a topographic feature map based on the flowchart in Figure 5, and (c) a global warming potential map of each topographic feature (Mg CO_2 eq/m^2) over the growing season.

pond portion of the potholes [cf. *Altor and Mitsch*, 2008; *Matson et al*., 2009]; in many cases, cumulative CH_4 effluxes in higher elevation features were negative, indicating consumption of atmospheric CH_4. Cumulative N_2O effluxes were generally largest in the moderately wet FS and TS features, consistent with previous research that observed increased denitrification rates in moderately wet soil conditions [e.g., *Corre et al*., 1999; *Dunmola et al*., 2010]. For the inundated pond portion of the potholes, the cumulative N_2O effluxes were negative, suggesting that when saturated or inundated portions of the pothole become anoxic, they reduce N_2O to N_2, becoming N_2O sinks [*Chapuis-Lardy et al*., 2007]. *Pennock et al*. [2010] observed small levels of N_2O emission in saturated mineral potholes in the Canadian prairie pothole region with larger levels as wetlands dried out. Cumulative N_2O effluxes were smaller than what is found in agriculturally impacted areas [*Corre et al*. 1999; *Yates et al*., 2006; *Phillips and Beeri*, 2008] irrespective of the position of the parcels along the coarse-scale climate gradient [*Phipps*, 2006; *Matson et al*., 2009]. This is likely because the natural potholes used in this study are not impacted by agricultural activities that use nitrogen fertilizers.

[42] Hydrologic profiles were found to control the heterogeneity of greenhouse gas fluxes. Previous studies in more rugged topographies showed the importance of taking a topographically based sampling design to improve estimates of greenhouse gas efflux [e.g., *Webster et al*., 2008]. Herein, we show the importance in a topographically based sampling design even in relatively subtle topography. If we were to assume that this subtle relief could be treated as topographically homogeneous, substantial overestimate and underestimate in greenhouse gas fluxes would occur. For example, when a parcel is assumed to be a uniform unit of land (represented by BS), CO_2 global warming potential was overestimated by as much as 20%, while CH_4 global warming potential was underestimated by as much as 100%. As models approached a more complete topography, from a single feature to multiple positions along pothole basin hillslopes, the magnitudes of the overestimate or underestimate decreased. These features define controls on greenhouse gas effluxes, demonstrating the effectiveness of

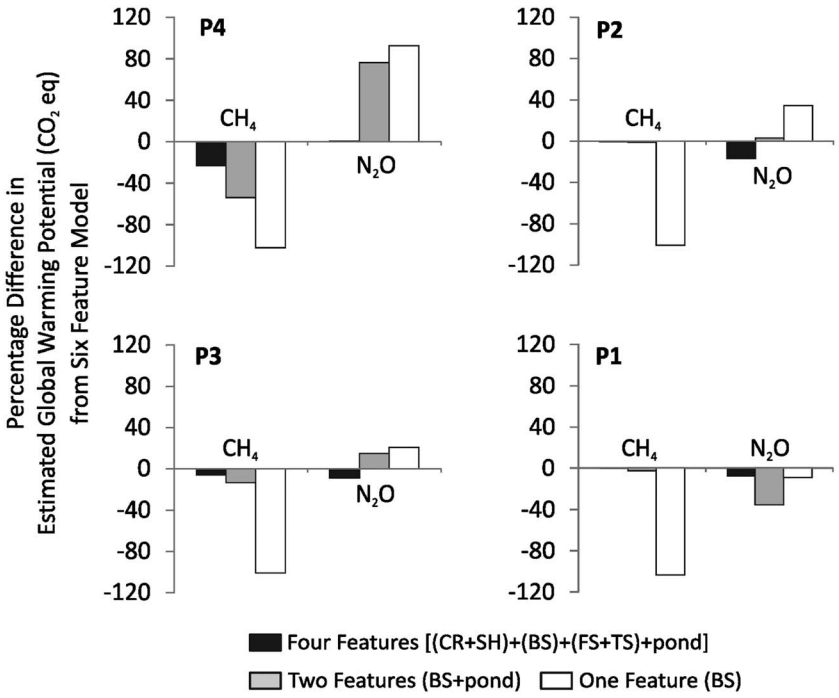

Figure 12. Comparison of the sensitivity of global warming potential estimates from the finest possible spatial aggregation scheme of land [CR, SH, BS, FS, and TS] and pond to different spatial aggregation schemes (four features: uplands (CR + SH), backslopes (BS), lowlands (FS + TS), and pond; two features: land [BS] and pond; and one feature: land only [BS]).

digital terrain analysis techniques for characterizing greenhouse gas cycling at fine spatial scales.

[43] Cumulative soil effluxes exhibited an increasing trend toward lower topographic features for CO_2 and a peak at TS for CH_4 in the northerly parcels (P3 and P4), although cumulative soil N_2O effluxes were relatively homogeneous across topographic features. Peak cumulative CH_4 and minimum cumulative CO_2 and N_2O effluxes were found in the inundated portions of ponds. *Webster et al.* [2011] suggested that soil sampling schemes based on random or regular spacing capture the most common topographic features on a landscape but may underestimate rare features. These features, although comprising a small portion of the landscape, may represent disproportionately higher rates of greenhouse gas formation than other areas on the landscape [*McClain et al*., 2003]. To detect these small but potentially important features, there is a need to design a spatially explicit topographic template that identifies areas with similar hydrologic and associated greenhouse gas activities [*Webster et al*., 2011]. Our study shows that the often subtle hydrologic profiles that characterize prairie potholes are important in estimating and explaining the spatial distribution of (or landscape heterogeneity in) soil greenhouse gas efflux.

[44] This paper provides support for our conceptual understanding of topographical controls on hydrology and associated greenhouse gas emissions within topographically subtle landscapes. The focus of this paper is on static hydrologic controls and does not consider within and among year dynamics. To capture real-time hydrologic profile dynamics, digital terrain analyses should be coupled with remote sensing techniques [cf. *Creed and Sass*, 2011; *Sass and Creed*, 2011]. Soil moisture is highly variable in time as well as in space, requiring dedicated sampling efforts in addition to a careful spatial strategy. The regular intervals of satellite-based radar imagery suggests an opportunity for temporal mapping of soil moisture [e.g., *Gala et al*., 2011] but requires investigation of the downscaling of coarse archived radar imagery to the small spatial scale of most topographic features [e.g., *Kaheil and Creed*, 2009]. The potential of coupling digital terrain analysis and remote sensing techniques to enable dynamic mapping of soil moisture dynamics is particularly important in the prairie pothole region because the region is expected to be strongly affected by climate change.

[45] As we consider the potential role of the prairie pothole region in global warming potential, we observed that the area contributing the largest greenhouse gas fluxes narrowed from the broader, relatively wet FS and TS lowland features of basins in P4 to the TS features only in P1. This suggests that the contributing source areas of greenhouse gas emissions are responsive to climatic conditions and that there is the potential that these areas would expand under wetter and contract under drier conditions. By extension, this also suggests that contributing source areas of greenhouse gas efflux will be expected to decrease under anticipated future climate conditions [*Millett et al*., 2009]. The potential for drought conditions on northern ecosystems is greatest for grasslands [*Johnson et al*., 2010; *Zha et al*., 2010]. Because a drier summer climate is anticipated in the prairie pothole region as a result of climate change, the gradient represented in this study can be expected to move northward, and with CO_2 and CH_4 fluxes decreasing in drier environments, without predictable increases or decreases in N_2O fluxes for these natural wetlands. The global warming

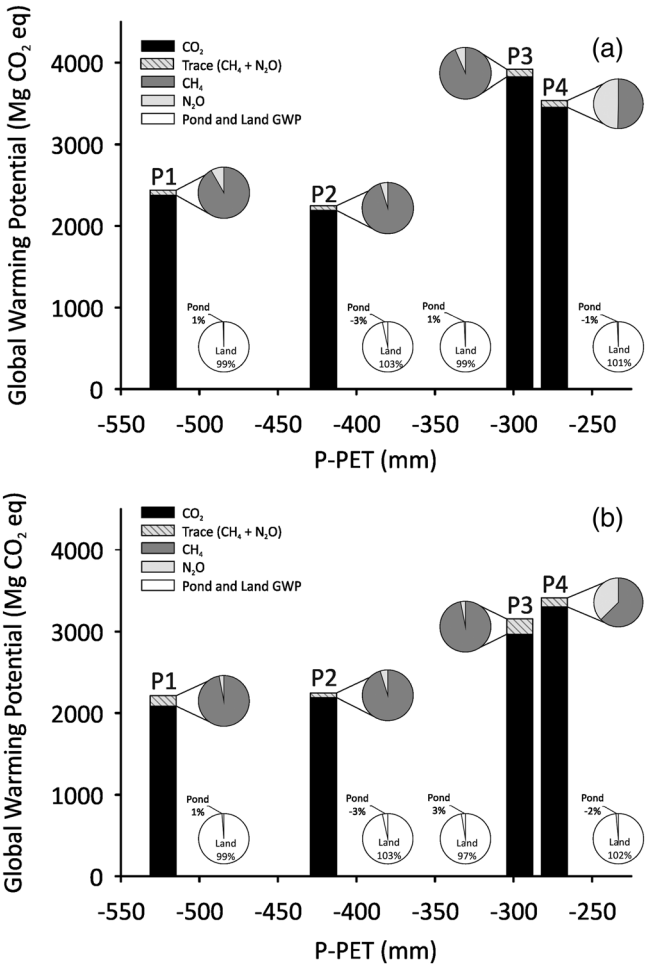

Figure 13. P-PET versus global warming potential (Mg CO_2 equivalent/per parcel/per growing season): (a) topographic feature areas for each parcel and (b) topographic feature areas standardized to P2 to remove the effect of inherent differences in topography among the parcels. Pie charts show relative contributions of trace gases as well as land and pond features to accumulated total global warming potential.

potential gains from restoring wetlands as reported by *Badiou et al*. [2011] may not end up being realized because the climatic conditions will have changed.

6. Conclusion

[46] Hydrology is an important control on greenhouse gas emissions in wetland basins in the prairie pothole region. Hydrologic controls are not uniformly distributed on the prairie landscape, with peak emissions of different greenhouse gases occurring under different hydrologic conditions. Greenhouse gas efflux sampling strategies that do not consider the spatial differences in hydrologic control may lead to under or overestimates of global warming potential due to greenhouse gas emissions. Greenhouse gas efflux sampling strategies that incorporate topographical proxies for hydrology improve estimates of greenhouse gas fluxes and associated global warming potential. Under current climatic conditions, CO_2 emissions account for more than 95% of global warming potential and are generally largest in the lowlands near ponds. CH_4 emissions are greatest in open water and can be a large component of global warming potential in low and wet landscape positions. N_2O emissions are important in natural wetlands. Averaging the greenhouse gas emissions of different features along the hillslope affected flux estimates: the number of features necessary is dependent on how much uncertainty one is willing to accept; with each reduction from six to four to two features, there were systematic changes in the estimated fluxes. The global warming potential of soil emissions tracks with hydrology from south to north along a climatic gradient, with smaller soil emissions expected with reduced water availability as the gradient moves northward due to anticipated climate change in the prairie pothole region.

Appendix A

[47] The six terrain attributes described in section 3.1 were used in a hierarchical fuzzy classification of topographic features from DEMs. For each rule in the classification hierarchy, fuzzy scores of terrain attributes were modeled in sigmoidal membership functions (*f*) increasing (inc) from no (0) membership to full (1) membership or decreasing (dec) from 1 to 0. An increasing function is used when membership is assumed to increase with increasing attribute values. The transitions in membership functions are governed by a central concept value (b) where membership is 0.5 and a dispersion index (d) with a value equal to the distance between full membership and the central concept value. Figure A1 summarizes the arithmetic combinations of fuzzy membership values into fuzzy scores and the hierarchy of decision rules used to assign topographic features to the fuzzy scores. Each rule assigns a topographic feature to a fuzzy score or passes the DEM grid cell unassigned to the next rule.

[48] In Rule 1, three terrain attributes were used to classify CR features, and terrain attribute values were converted from "crisp" or untransformed values to fuzzy values:

CR1 = percent height relative to local channels and divides (*f* inc; b = 70; d = 20)
CR2 = slope (*f* dec; b = 2.4; d = 0.9)
CR3 = plan curvature (*f* dec; b = −6; d = 6)

[49] The three fuzzy membership maps were multiplied together, and pixels with a value greater than 0.33 were classified as CR; remaining pixels were passed on to the next rule.

[50] Uplands (BS and SH) were separated from lowlands (FS and TS) in Rule 2. Three terrain attributes were used to classify uplands (UP) and lowlands (LOW):

UP1 = wetness index (*f* dec; b = 6.2; d = 0.9)
LOW1 = wetness index (*f* inc); b = 6.4; d = 1.4)
UP2 = percent height relative to local pits and peaks (*f* inc; b = 22; d = 16)
LOW2 = percent height relative to pits and peaks (*f* decd; b = 21; d = 12)
UP3 = slope (*f* inc; b = 5.3; d = 4)
LOW3 = slope (*f* dec; b = 7.6; d = 4)

[51] The three UP fuzzy membership maps were multiplied together, and pixels with a value greater than the

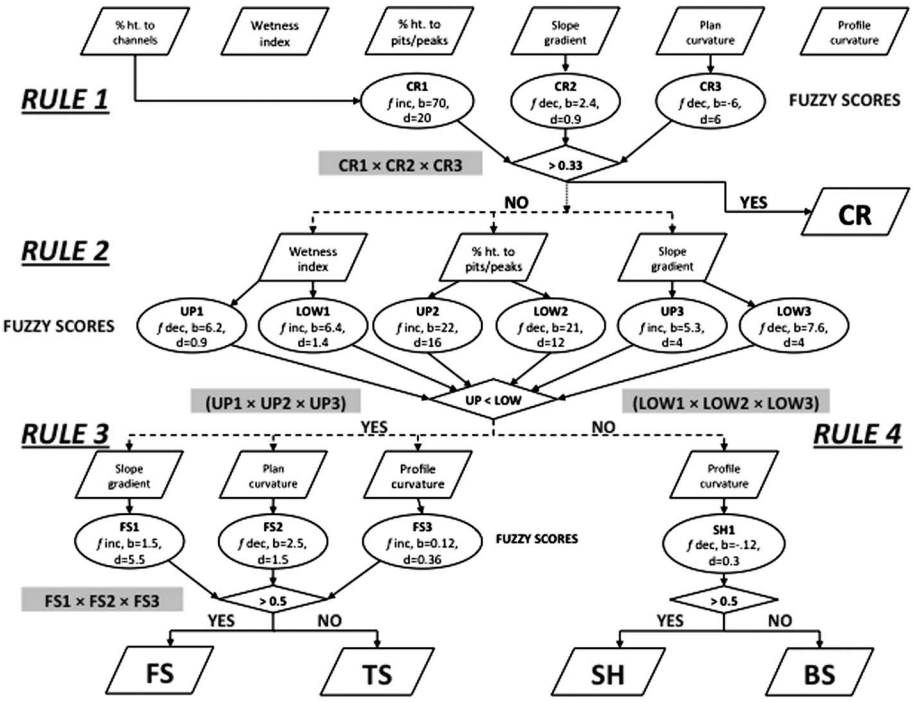

Figure A1. Flowchart of steps for classifying topographic features from terrain attributes.

product of the three LOW fuzzy membership maps multiplied together were classified as UP; remaining pixels were classified as LOW.

[52] In Rule 3, three terrain attributes were used to separate LOW features into FS and TS features:

FS1 = slope (*f* inc; b = 1.5; d = 5.5)
FS2 = plan curvature (*f* dec; b = 2.5; d = 1.5)
FS3 = profile curvature (*f* inc; b = 0.2; d = 0.36)

[53] The three fuzzy membership maps were multiplied together, and pixels with a value greater than 0.5 were classified as FS; remaining pixels were classified as TS.

[54] In Rule 4, one terrain attribute was used to separate UP features into SH and BS features:

SH1 = profile curvature (*f* dec; b = −0.12; d = 0.3)

[55] Features with a value greater than 0.5 were classified as SH; remaining pixels were classified as BS.

[56] **Acknowledgments.** This study was funded by NSERC (Discovery Grant to IFC), Ducks Unlimited Canada (Grant to IFC, RAB), and through Environment Canada's participation in the Program for Energy Research & Development (RAB). T. Malakoff and S. Kelly provided exceptional service in the installation of the boardwalks and the instrumentation, monitoring, and sampling of the potholes. K. Edmondson provided assistance with the chemical and gas chromatographic analyses, and F. Dunnett designed and constructed the collars and chambers used for greenhouse gas efflux determination.

References

Altor, A. E., and W. J. Mitsch (2008), Pulsing hydrology, methane emissions and carbon dioxide fluxes in created marshes: A 2-year ecosystem study, *Wetlands*, *28*, doi:10.1672/07-98.1.

Badiou, P., R. McDougal, D. Pennock, and B. Clark (2011), Greenhouse gas emissions and carbon sequestration potential in restored wetlands of the Canadian prairie pothole region, *Wetl. Ecol. Manag.*, *19*, doi:10.1007/s11273-011-9214-6.

Beven, K., and M. J. Kirkby (1979), A physically based, variable contributing area model of basin hydrology, *Hydrol. Sci. Bull.*, *24*, 43–69, doi:10.1080/02626667909491834.

Bridgham, S. D., J. P. Megonigal, J. K. Keller, N. B. Bliss, and C. Trettin (2006), The carbon balance of North American wetlands, *Wetlands*, *26*, doi:10.1672/0277-5212(2006)26[889:TCBONA]2.0.CO;2.

Brye, K. R., and E. E. Gbur (2010), Regional differences in soil carbon and nitrogen storage as affected by land use and soil moisture regime, *Soil Sci.*, *175*, doi:10.1097/SS.0b013e3181e83db2.

Carlyle, S. A. (2006), Changing nature of topographic control on surface soil moisture of prairie pothole complexes along a climate gradient, MSc Thesis, Dep. of Geog., Univ. of Western Ontario, London, Ontario, Canada.

Chapuis-Lardy, L., N. Wrage, A. Metay, J.-L. Chottes, and M. Bernoux (2007), Soils, a sink for N2O? A review, *Global Change Biol.*, *13*, doi:10.1111/j.1365-2486.2006.01280.x.

Corre, M. D., D. J. Pennock, C. Van Kessel, and D. K. Elliott (1999), Estimation of annual nitrous oxide emissions from a transitional grassland-forest region in Saskatchewan, Canada, *Biogeochemistry*, *44*, 29–49, doi:10.1007/BF00992997.

Creed, I. F., and G. Z. Sass (2011), Digital terrain analysis approaches for tracking hydrological and biogeochemical pathways and processes in forested landscapes, in *Forest Hydrology and Biogeochemistry*: *Synthesis of Past Research and Future Directions*, edited by D. F. Levia, D. E. Carlyle-Moses, T. Tanaka, pp. 69–100, Springer-Verlag, Heidelberg, Germany, doi:10.1007/978-94-007-1363-5_4.

Dunmola, A. S., M. Tenuta, A. P. Moulin, P. Yapa, and D. A. Lobb (2010), Pattern of greenhouse gas emission from a Prairie Pothole agricultural landscape in Manitoba, Canada, *Can. J. Soil Sci.*, *90*, doi:10.4141/CJSS08053.

Environment Canada (1986), Wetlands in Canada: A valuable resource. Fact Sheet 86–4, 8pp, Lands Directorate, Ottawa, Ontario.

Euliss, N. H., R. A. Gleason, A. Olness, R. L. McDougal, H. R. Murkin, R. D. Robarts, R. A. Bourbonniere, and B. G. Warner (2006), North American prairie wetlands are important nonforested land-based carbon storage sites, *Sci. Total Environ.*, *361*, doi:10.1016/j.scitotenv.2005.06.007.

Forster, P. et al. (2007), Changes in atmospheric constituents and in radiative forcing, in *Climate Change 2007: The Physical Science Basis, Contribution of Working Group I to the Fourth Assessment Report of the Intergovernmental Panel on Climate Change*, edited by S. Solomon, D. Qin, M. Manning, Z. Chen, M. Marquis, K. B. Averyt, M. Tignor and H. L. Miller, pp. 129–204, Cambridge University Press, Cambridge, United Kingdom and New York, NY, USA.

Fung, K. I. (1969a), Bedrock geology. In *Atlas of Saskatchewan*, edited by J. H. Richards and K. Fung, pp. 40–41. University of Saskatchewan, Saskatoon, Saskatchewan, Canada.

Fung, K. I. (1969b) Natural vegetation. In *Atlas of Saskatchewan*, edited by J. H. Richards, p. 263. University of Saskatchewan, Saskatoon, Saskatchewan, Canada.

Gala, T. S., D. A. Aldred, S. Carlyle, and I. F. Creed (2011), Topographically based spatially averaging of SAR data improves performance of soil moisture models. *Remote Sens. Environ.*, *115*, doi:10.1016/j.rse.2011.08.013.

Gleason, R. A., B. A. Tangen, B. A. Browne, and N. H. Euliss (2009), Greenhouse gas flux from cropland and restored wetlands in the Prairie Pothole Region, *Soil Biol. Biochem.*, *41*, doi:10.1016/j.soilbio.2009.09.008.

Hamon, W. R. (1961), Estimating potential evapotranspiration, *J. Hydraulics. Div.-ASCE*, *87*.

Johnson, W. C., B. Werner, G. R. Guntenspergen, R. A. Voldseth, B. Millett, D. E. Naugle, M. Tulbure, R. W. H. Carroll, J. Tracy, and C. Olawsky (2010), Prairie wetland complexes as landscape functional units in a changing climate, *Bioscience*, *60*, doi:10.1525/bio.2010.60.2.7.

Kaheil, Y. H., and I. F. Creed (2009), Detecting and downscaling wet areas on boreal landscapes. *IEEE Geosci. Remote S.*, *6*, doi:10.1109/LGRS.2008.2010001.

van der Kamp, G., and M. Hayashi (2009), Groundwater-wetland ecosystem interaction in the semiarid glaciated plains of North America, *Hydrogeol. J.*, *17*, doi:10.1007/s10040-008-0367-1.

Lindsay, J. B (2005), The Terrain Analysis System: A tool for hydro-geomorphic applications, *Hydrol. Process*, *19*, doi:10.1002/hyp.5818.

Livingston G. P., and G. L. Hutchinson (1995), Enclosure-based measurement of trace gas exchange: Applications and sources of error, in *Biogenic Trace Gases: Measuring Emissions from Soil and Water*, edited by P. A. Matson and R. C. Harris, pp. 14–51, Blackwell Science Inc., Cambridge, MA, USA.

MacMillan, R. A (2000), A protocol for preparing digital elevation (DEM) data for input and analysis using the landform segmentation model (LSM) programs, Soil Variability Analysis to Enhance Crop Production (SVAECP) Project.

Matson, A., D. Pennock, and A. Bedard-Haughn (2009), Methane and nitrous oxide emissions from mature forest stands in the boreal forest, Saskatchewan, Canada, *For. Ecol. Manag.*, *258*, doi:10.1016/j.foreco.2009.05.034.

McClain, M. E., et al. (2003), Biogeochemical hot spots and hot moments at the interface of terrestrial and aquatic ecosystems, *Ecosystems*, *6*, doi:10.1007/s10021-003-0161-9.

Millett, B., W. C. Johnson, and G. Guntenspergen (2009), Climate trends of the North American prairie pothole region 1906–2000, *Clim. Chang.*, *93*, 243–267, doi:10.1007/s10584-008-9543-5.

Mitsch, W. J., and J. G. Gosselink (2000), *Wetlands—3rd Ed.*, John Wiley & Sons, New York.

Nelson, J. D. J., J. J. Schoenau, and S. S. Malhi (2008), Soil organic carbon changes and distribution in cultivated and restored grassland soils in Saskatchewan, *Nutr. Cycl. Agroecosys.*, *82*, doi:10.1007/s10705-008-9175-1.

Niemuth, N. D., B. Wangler, and R. E. Reynolds (2010), Spatial and temporal variation in wet area of wetlands in the Prairie Pothole Region of North Dakota and South Dakota, *Wetlands*, *30*, doi:10.1007/s13157-010-0111-1.

O'Callaghan, J. F., and D. M. Mark (1984), The extraction of drainage networks from digital elevation data, *Comput. Vision Graph.*, *28*, 323–344, doi:10.1016/S0734-189X(84)80011-0.

Pennock, D. (2007), *The Agriculture and Wetlands Greenhouse Gas Initiative (AWGI): Overview of Projects Within the Initiative and Research Summary*, Ducks Unlimited Canada—Institute for Wetlands and Waterfowl Research, Stonewall, MB, Canada, 16pp.

Pennock, D. J., B. J. Zebarth, and E. Dejong (1987), Landform classification and soil distribution in hummocky terrain, Saskatchewan, Canada, *Geoderma*, *40*, 297–315, doi:10.1016/0016-7061(87)90040-1.

Pennock, D., T. Yates, A. Bedard-Haughn, K. Phipps, R. Farrell, and R. McDougal (2010), Landscape controls on N2O and CH4 emissions from freshwater mineral soil wetlands of the Canadian Prairie Pothole region, *Geoderma*, *155*, doi:10.1016/j.geoderma.2009.12.015.

Phillips, R., and O. Beeri (2008), The role of hydropedologic vegetation zones in greenhouse gas emissions for agricultural wetland landscapes, *Catena*, *72*, doi:10.1016/j.catena.2007.07.007.

Phipps, K. J. (2006), Spatial and temporal variation in greenhouse gas emissions from two open water prairie wetlands, MSc Thesis, Dep. of Soil Sci., Univ. of Saskatchewan, Saskatoon, Saskatchewan, Canada.

Planchon, O., and F. Darboux (2002), A fast, simple and versatile algorithm to fill the depressions of digital elevation models, *Catena*, *46*, doi:10.1016/S0341-8162(01)00164-3.

Sass, G. Z., and I. F. Creed (2011), Bird's eye view of forest hydrology: Novel approaches using remote sensing techniques, in *Forest Hydrology and Biogeochemistry: Synthesis of Past Research and Future Directions*, edited by D. F. Levia, D. E. Carlyle-Moses, T. Tanaka, pp. 45–68, Springer-Verlag, Heidelberg, Germany, doi:10.1007/978-94-007-1363-5_3.

Scott, G. A. J. (1995), *Canada's Vegetation: A World Perspective, 361 pp.*, McGill-Queen's University Press, Montreal.

Shieflo, J. B. (1968), *Evapotranspiration and the Water Budget of Prairie Potholes in North Dakota, Paper 585-B*, US Geological Survey, Reston, Virginia.

Soil Landscapes of Canada Working Group (2010), Soil landscapes of Canada version 3.2. Agriculture and Agri-Food Canada. (digital map and database at 1:1 million scale).

Systat Software Inc. (2011), SigmaPlot, Version 12.0 for Windows.

Tang, J., and D. D. Baldocchi (2005), Spatial-temporal variation in soil respiration in an oak-grass savanna ecosystem in California and its partitioning into autotrophic and heterotrophic components, *Biochemistry*, *73*, doi:10.1007/s10533-004-5889-6.

Tarboton, D. G. (1997), A new method for the determination of flow directions and upslope areas in grid digital elevation models, *Water Resour. Res.*, *33*, 309–319, doi:10.1029/96WR03137.

Tiner, R. W. (2003), Geographically isolated wetlands of the United States, *Wetlands*, *23*, doi:10.1672/0277-5212(2003)023[0494:GIWOTU]2.0.CO;2.

van der Valk, A. G., and R. L. Pederson (2003), The SWANCC decision and its implications for prairie potholes, *Wetlands*, *23*, doi:10.1672/0277-5212(2003)023[0590:TSDAII]2.0.CO;2.

Waiser, M. J. (2006), Relationship between hydrologic characteristics and dissolved organic carbon concentration and mass in northern prairie wetlands using a conservative tracer approach, *J. Geophys. Res.-Biogeo.*, *111*, G02024, doi:10.1029/2005JG000088.

Webster, K. L., I. F. Creed, F. D. Beall, and R. A. Bourbonniere (2008), Controls on the heterogeneity of soil respiration in a tolerant hardwood forest, *J. Geophys. Res.-Biogeo.*, *113*, G03040, doi:10.1029/2008JG000706.

Webster, K. L., I. F. Creed, M. D. Skowronski, and Y. H. Kaheil (2009), Comparison of the performance of statistical models that predict soil respiration from forests, *Soil Sci. Soc. Am. J.*, *73*, doi:10.2136/sssaj2008.0310.

Webster, K. L., I. F. Creed, F. D. Beall, and R. A. Bourbonniere (2011), A topographic template for estimating soil carbon pools in forested landscapes, *Geoderma*, *160*, doi:10.1016/j.geoderma.2010.10.016.

Wilson, J., and J. C. Gallant (2000), *Terrain Analysis: Principles and Applications*, Wiley, New York.

Winter, T. C., and J. W. LaBaugh (2003), Hydrologic considerations in defining isolated wetlands, *Wetlands*, *23*, doi:10.1672/0277-5212(2003)023[0532:HCIDIW]2.0.CO;2.

Winter, T. C., and D. O. Rosenberry (1998), Hydrology of prairie pothole wetlands during drought and deluge: A 17-year study of the cottonwood lake wetland complex in North Dakota in the perspective of longer term measured and proxy hydrologic records, *Clim. Chang.*, *40*, 189–209, doi:10.1023/A:1005448416571.

Yates, T. T., B. C. Si, R. E. Farrell, and D. J. Pennock (2006), Probability distribution and spatial dependence of nitrous oxide emission: Temporal change in hummocky terrain, *Soil Sci. Soc. Am. J.*, *70*, doi:10.2136/sssaj2005.0214.

Zha, T. S., A. G. Barr, G. van der Kamp, T. A. Black, J. H. McCaughey, and L. B. Flanagan (2010), Interannual variation of evapotranspiration from forest and grassland ecosystems in western Canada in relation to drought, *Ag. For. Meteorol.*, *150*, doi:10.1016/j.agrformet.2010.08.003.